Efficient Energy and Electron Transfer Photocatalysis with a Coulombic Dyad

Matthias Schmitz [a], Maria-Sophie Bertrams [a], Arne C. Sell [a], Felix Glaser [a, b], and Christoph Kerzig [a]*

[a] *Department of Chemistry, Johannes Gutenberg University Mainz, Duesbergweg 10–14, 55128 Mainz, Germany*
[b] *Present Address: Université catholique de Louvain (UCLouvain), Institute of Condensed Matter and Nanosciences (IMCN), Molecular Chemistry, Materials and Catalysis (MOST), Place Louis Pasteur 1, bte L4.01.02, 1348 Louvain-la-Neuve, Belgium*

* Email: ckerzig@uni-mainz.de

Abstract: *Photocatalysis holds great promise for changing the way how value-added molecules are currently prepared. However, many photocatalytic reactions suffer from lousy quantum yields, hampering the transition from lab-scale reactions to large-scale or even industrial applications. Molecular dyads can be designed such that the beneficial properties of inorganic and organic chromophores are combined, resulting in milder reaction conditions and improved quantum yields of photocatalytic reactions. We have developed a novel approach for obtaining the advantages of molecular dyads without the time- and resource-consuming synthesis of these tailored photocatalysts. Simply by mixing a cationic ruthenium complex with an anionic pyrene derivative in water a salt bichromophore is produced owing to electrostatic interactions. The long-lived organic triplet state is obtained by static and quantitative energy transfer from the preorganized ruthenium complex. We exploited this so-called Coulombic dyad for energy transfer catalysis with similar reactivity and even higher photostability compared to a molecular dyad and reference photosensitizers in several photooxygenations. In addition, it was shown that this system can also be used to maximize the quantum yield of photoredox reactions. This is due to an intrinsically higher cage escape quantum yield after photoinduced electron transfer for purely organic compounds compared to heavy atom-containing molecules. The combination of laboratory-scale as well as mechanistic irradiation experiments with detailed spectroscopic investigations provided deep mechanistic insights into this easy-to-use photocatalyst class.*

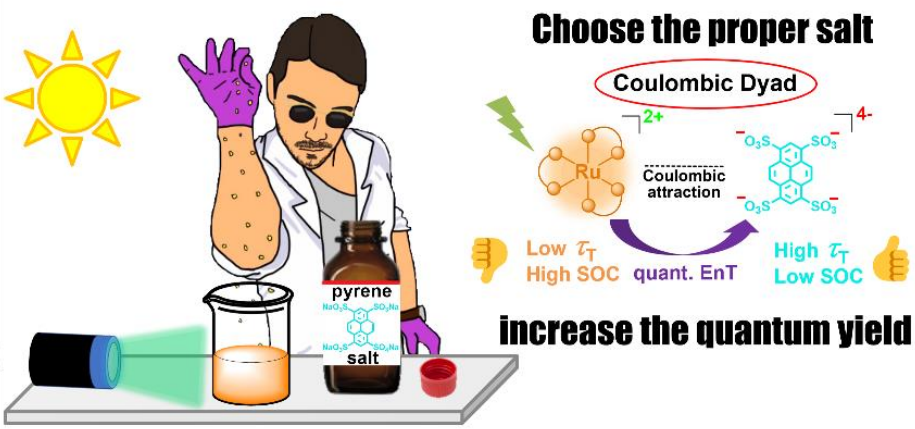

Introduction

Catalytic transformations of small molecules via photoredox[1–4] and energy transfer[5–7] catalysis represent a rapidly growing research field.[8,9] Scientists from several disciplines actively contributed to this impressive development and recent breakthroughs in the sub-disciplines mechanism development,[10–15] reaction engineering[16–18] and photocatalyst design[19–26] have been achieved. However, many or even most of the photocatalytic reactions reported so far have to rely on several hours of irradiation using high-power LEDs for transforming milligram quantities of given substrates, which already implies very low overall quantum yields. The reaction quantum yield is frequently overlooked in the design of novel photoreactions but this parameter will likely play a key role in the further development of industrially scalable photoreactions.[27] Deep mechanistic investigations using transient absorption (TA) spectroscopy are a powerful tool not only to differentiate between different mechanistic scenarios but also to optimize reaction steps and the overall reaction quantum yield.[28–32]

Metal complexes having $4d^6$ or $5d^6$ valence electron configurations with corresponding metal-to-ligand charge transfer (MLCT) states are among the best-investigated photocatalysts as a result of their beneficial properties including visible-light absorptivity, quantitative triplet formation and tunability.[2,33–35] However, their triplet state lifetimes are frequently too short for quantitative quenching via energy transfer (EnT) or electron transfer (ET) with a substrate or additive in a catalytic cycle.[36,37] Additionally, ET quenching suffers from unproductive in-cage recombination due to the heavy-atom effect and concomitant radical-pair intersystem crossing (ISC).[38–44] These issues reduce the achievable quantum yields for many photoreactions drastically. Tailor-made molecular dyads consisting of a metal complex (MC) unit and a covalently linked organic chromophore (OC)[45–47] have the potential to solve these efficiency problems owing to the long-lived and heavy-atom free organic triplet being accessible after intramolecular energy transfer (iEnT) from the photoexcited metal complex. Significantly improved quantum yields for EnT and ET key reaction steps in photocatalysis were observed when comparing dyads and parent metal complexes,[36,38,48–57] but the required multi-step syntheses of these improved bichromophoric photocatalysts hamper their broader usage.

Attractive and repulsive Coulomb interactions are among the most fundamental non-covalent interactions and it comes to no surprise that they have been used extensively to control the outcome of chemical reactions. Exploiting photocatalyst–quencher[58–69] Coulombic interactions is a well-established strategy for improving the efficiency of photochemical key steps and the reaction performance accordingly, either by accelerated diffusion between oppositely charged

species or by static quenching owing to pre-aggregation. Furthermore, underexplored counterion[70–74] as well as ion-pairing[60,75–78] effects received some attention from the photochemistry community in recent years. Herein, we demonstrate that the favorable properties of MC–OC dyads can be obtained by exploiting Coulombic attraction between commercially available ionic chromophores. As we will show, these readily accessible Coulombic dyads clearly outperform the catalytic reactivity of the parent ruthenium(II) and also osmium(II) complexes. Using several spectroscopic techniques and test reactions, we compare all key properties of a molecular and a Coulombic dyad based on a ruthenium-tris(diimine) unit as MC and a pyrene moiety as OC (Figure 1). Despite the ongoing development in preparing photoactive complexes based on Earth-abundant metals and recent breakthroughs in this field,[20–22,24–26,79,80] precious $4d^6$ and $5d^6$ metal complexes will most likely stay the workhorses for most photoreactions in the near future. Concepts significantly improving the performance of precious photoactive metal complexes that are easy to implement would thus have far-reaching implications.

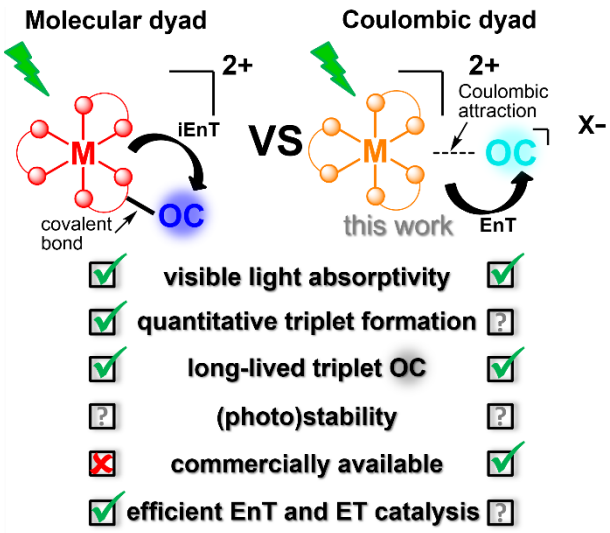

Figure 1 Comparison of key properties of well-known, tailor-made molecular MC–OC dyads and novel Coulombic dyads prepared by mixing commercially available chromophore-containing salts.

Results and Discussion

Dyad Design

Guided by our recent studies with a water-soluble molecular dyad comprising a ruthenium-tris(phenanthroline) (**Ruphen**) complex and a pyrene moiety,[36,57] hereafter referred to as **RuphenPy** (see Figure 2), we aimed at mimicking its photophysical and photochemical properties through intermolecular interactions without the necessity of a multi-step synthesis.

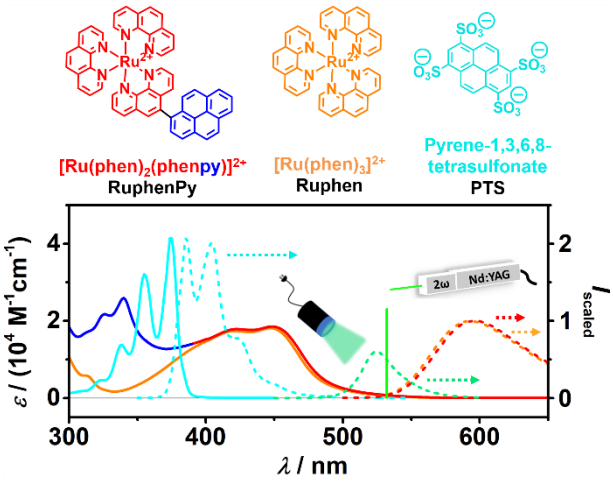

Figure 2 Molecular structures of the main compounds of this study, together with corresponding abbreviations, UV-vis absorption (solid line) and normalized emission spectra (dotted line). The spectra of the metal complexes (as chloride salts) and the pyrene-derivative (as sodium salt) were recorded in MilliQ water. The excitation wavelength for laser flash photolysis measurements (solid vertical line, λ_{exc} = 532 nm) and the emission spectrum of the LED used for lab-scale irradiation experiments (dotted green line, $\lambda_{exc,max}$ = 525 nm) are highlighted in the spectrum.

Dicationic **Ruphen** is intrinsically suitable for using Coulombic interactions – as numerous photoactive Ru, Ir and Os complexes are – to accelerate diffusion or to form a supramolecular complex with a negatively charged OC salt. Regarding the triplet-energy adapted pyrene,[47,57,63,81–87] the tetrasodium salt of pyrene-1,3,6,8-tetrasulfonic acid (**PTS**), a low-cost and commercially available compound with four negative charges, emerges as an ideal aggregation counterpart for **Ruphen**. **PTS** has been used in different fields, including the formation of charge transfer (CT) complexes,[88] aggregation with enzymes,[89] integration into 2D metal-organic frameworks,[90] and participation in self-assembling supramolecular systems.[91] All of these applications exploit the high charge density of **PTS**. In addition, **PTS** is also widely used as a fluorescence probe,[91,92] along with various other pyrene-based fluorophores.[93] Considering the typically low pK_a of aromatic sulfonic acids in water, it is very likely that **PTS** is predominantly present in its fully deprotonated state, maximizing the attractive Coulombic interactions with a positively charged sensitizer. Moreover, the water-soluble chloride salt of

the ruthenium complex is commercially available, allowing straightforward preparation of a Coulombic dyad of **Ruphen** and **PTS** by simply dissolving both salts in water.

Steady-State Absorption and Emission Properties

Ruphen exhibits a ^{1}MLCT absorption band in the visible region along with a ^{3}MLCT emission peaking at λ_{max} ~ 594 nm.[94] In the molecular dyad **RuphenPy**, the MLCT absorption and emission bands exhibit a slight red shift compared to those of **Ruphen**. This shift is due to minor changes in the ^{3}MLCT state energies caused by the covalently bound chromophore. The **RuphenPy** absorption spectrum is basically a superposition of the **Ruphen** and pyrene ground state absorption bands, confirming the presence of both chromophores (see Figure 2).[36] Dissolved **PTS** shows a characteristic fine-structured pyrene $^1(\pi\text{-}\pi)^*$ absorption band[92,95] located at the low-energy end of the UV spectrum. It also exhibits a fluorescence spectrum with a Stokes-shifted fluorescence profile that accurately reflects the absorption features.[92] Due to the presence of four sulfonic acid groups, the absorption and emission characteristics of **PTS** show a prominent red shift compared to the spectra of unmodified pyrene, which implies lower excited-state energies for **PTS**. Upon the addition of **PTS** to a solution containing **Ruphen**, a slight spectral broadening and a red shift of the MLCT absorption band become apparent, while solubility issues do not occur for micromolar and lower millimolar concentrations. This initial observation is a first indication of ground state aggregation involving both chromophores, which will be discussed in the next subsection.

Ground State Association and Energy Transfer between Ruphen and PTS

In the molecular dyad **RuphenPy** (see Figure 2 for its structure), the organic triplet state is produced through a sub-nanosecond intramolecular energy transfer from the ^{3}MLCT state as the energy donor.[36] This transfer leads to the formation of a $^3(\pi\text{-}\pi)^*$ state almost exclusively localized on the pyrene moiety. To explore whether a similar phenomenon in the charge-adapted **Ruphen**–**PTS** pair takes place, a classical Stern–Volmer experiment was performed investigating the quenching of the emissive ^{3}MLCT state upon the addition of **PTS** (see Figure 3 (a)). The experiments reveal distinct quenching characteristics for the charge-adapted Dexter energy transfer pair: A shortening of the ^{3}MLCT lifetime and a simultaneous decrease in the initial emission intensity. The shorter lifetime of the ^{3}MLCT state is attributed to dynamic, *i.e.* diffusion-based, quenching between dicationic ^{3}**Ruphen** and tetraanionic **PTS**. The calculated quenching rate constant, $k_q = 2.5 \cdot 10^{10}$ $M^{-1}s^{-1}$, clearly exceeds the conventional diffusion limit in an aqueous medium ($6.5 \cdot 10^9$ $M^{-1}s^{-1}$)[95]. This pronounced difference is rationalized by

Coulombic attraction between **Ruphen** and **PTS**, which effectively accelerates the dynamic quenching process. For entirely diffusion-controlled quenching, the amount of ^{3}MLCT states generated following laser pulses of constant energy would remain constant regardless of the amount of quencher present, leading to identical initial emission amplitudes. However, we observed a decrease in the initial emission amplitude that correlates with the amount of **PTS** present, indicating the occurrence of quasi-instantaneous (on a sub-ns timescale) static quenching. In molecular dyads, spatial proximity is ensured through covalent bonds, which enable rapid *intramolecular* energy transfer processes. A similar process with predominantly static quenching is seemingly achieved through strong attractive interactions[96,97] in the Coulombic dyad, resulting in *intra-ion-pair* energy transfer. Comparative investigations with pyrene monosulfonic acid (**PMS**, monoanionic) and uncharged pyrene (see SI, section S4) showed less pronounced static quenching and the complete absence of static quenching, respectively. These observations indicate that electrostatic interactions are in charge for the prominent static quenching phenomenon.

To provide clear evidence for ion-pairing, an NMR titration[98,99] experiment (see section S2.2 in the SI) was carried out, which revealed that **Ruphen** and **PTS** aggregate predominantly in a 1:1 ratio. Based on this result and considering that the **Ruphen** molar absorption coefficient is essentially identical in the aggregate at our excitation wavelengths (see also section S2.1 of the SI), we employed the conventional equation for quantifying static quenching[97] in combination with the initial emission intensity, which leads to an association constant of $K_s = 6.1 \cdot 10^4$ M^{-1}. Gratifyingly, both static and dynamic quenching contributions show a linear trend in the Stern–Volmer plot (see inset in Figure 3 (a)). Moreover, a textbook-like quadratic trend is evident when the total emission intensity is used as the basis for the Stern–Volmer plot, as illustrated by the black curve. This result is consistent with the expected behavior for mixed dynamic and static quenching.[97] The quadratic dependency is also obtained in steady-state emission quenching measurements, as explained in more detail in the SI (section S2.3). However, to separate the effects of static and dynamic quenching, it is mandatory to utilize time-resolved measurements. The high constants for dynamic and static quenching enable almost quantitative quenching (> 95%) of ^{3}**Ruphen** already at **PTS** concentrations as low as 90 µM (88% static quenching, 9% dynamic quenching).

Detailed TA studies with our nanosecond laser flash photolysis (LFP) setup[71] (see SI for details) were carried out to obtain clear evidence for the underlying quenching mechanism and to exclude undesired reaction pathways. After complete quenching, the TA spectrum exhibit the

characteristic features of the **PTS** triplet state (see Figure 3 (b)).[100–102] The formation of **PTS**-derived radical ions that could result from photoinduced electron transfer quenching can be excluded with the literature-known reference spectra.[100,101] The same results are obtained for the molecular dyad **RuphenPy**, where the $^3(\pi\text{-}\pi)^*$ state is populated immediately after selective excitation of the Ru complex unit.[36] Figure 3 (c) shows the TA data sets monitored at the isosbestic point of **Ruphen** and its triplet **^{3}Ruphen** (496 nm), allowing the observation of the newly formed species **^{3}PTS** in isolation. Immediately after the laser pulse, an increase in the transient absorption signal of **^{3}PTS** can be detected due to the productive static quenching process. This is followed by a much slower increase in absorption attributed to the **^{3}PTS** formation *via* dynamic quenching. The relative contributions of dynamic and static quenching to the formation of **^{3}PTS** closely mirror their roles in the overall emission quenching efficiencies, suggesting a highly efficient energy transfer mechanism from **^{3}Ruphen** to **PTS**. Quantitative LFP measurements[39,103] using the molar absorption coefficients of the excited states indicate that this initial energy transfer process proceeds with a near-quantitative quantum yield of 0.94 under our conditions using 120 µM of **PTS** (see sections S7 and S8.1 in the SI). Millimolar concentrations of a pyrene derivative would be required without exploiting attractive electrostatic interactions and the resulting ion-pairing for achieving similar efficiencies.[63,86]

The pyrene triplet state has an elongated triplet lifetime due to the much lower spin-orbit coupling compared to the ruthenium complex.[95] For the molecular dyad, a lifetime of the mainly pyrene-localized triplet on the order of 50 µs is achieved (see ref. [36] and Figure 4). However, for **PTS**, an even longer triplet lifetime, of 355 µs is detected (Figure 4). This can be explained by the absence of back energy transfer to the inorganic chromophore. In the molecular dyad, the energy difference between the $^3(\pi\text{-}\pi)^*$ and ^{3}MLCT states is only about 0.1 eV,[36] resulting in a thermally activated intramolecular back energy transfer, depopulation the $^3(\pi\text{-}\pi)^*$ state on a microsecond timescale. **PTS**, on the other hand, bears four sulfonate groups, significantly lowering its triplet energy as confirmed by 77 K phosphorescence measurements of **PTS**, which gave a triplet energy of 1.80 eV (see SI, section S10.1), and DFT calculations that predict the **PTS** triplet at 1.85 eV (see SI, section S10.2). This leads to an energy difference of about 0.4 eV between **^{3}Ruphen** and **^{3}PTS** rendering uphill back energy transfer infeasible under the given conditions.[104] Consequently, a purely pyrene-localized triplet is present in the Coulombic dyad, while the molecular dyad under study serves as a triplet reservoir.[36,47] The formation of the pyrene triplets for the molecular or the Coulombic dyad is briefly summarized in Figure 3 (d). After visible-light excitation, the ruthenium complex units undergo quantitative ISC.

Subsequently, quenching efficiencies of up to 100% can be achieved either by *intramolecular* energy transfer (**RuphenPy**) or by highly efficient *ion-pair* and additional *intermolecular* dynamic energy transfer processes (Coulombic dyad). Hence, almost every photon harvested by the ruthenium complex leads to the generation of a long-lived organic triplet state, which would not be possible with harmful UV light sources upon direct pyrene excitation owing to inefficient ISC and side reactions.[95,100,101]

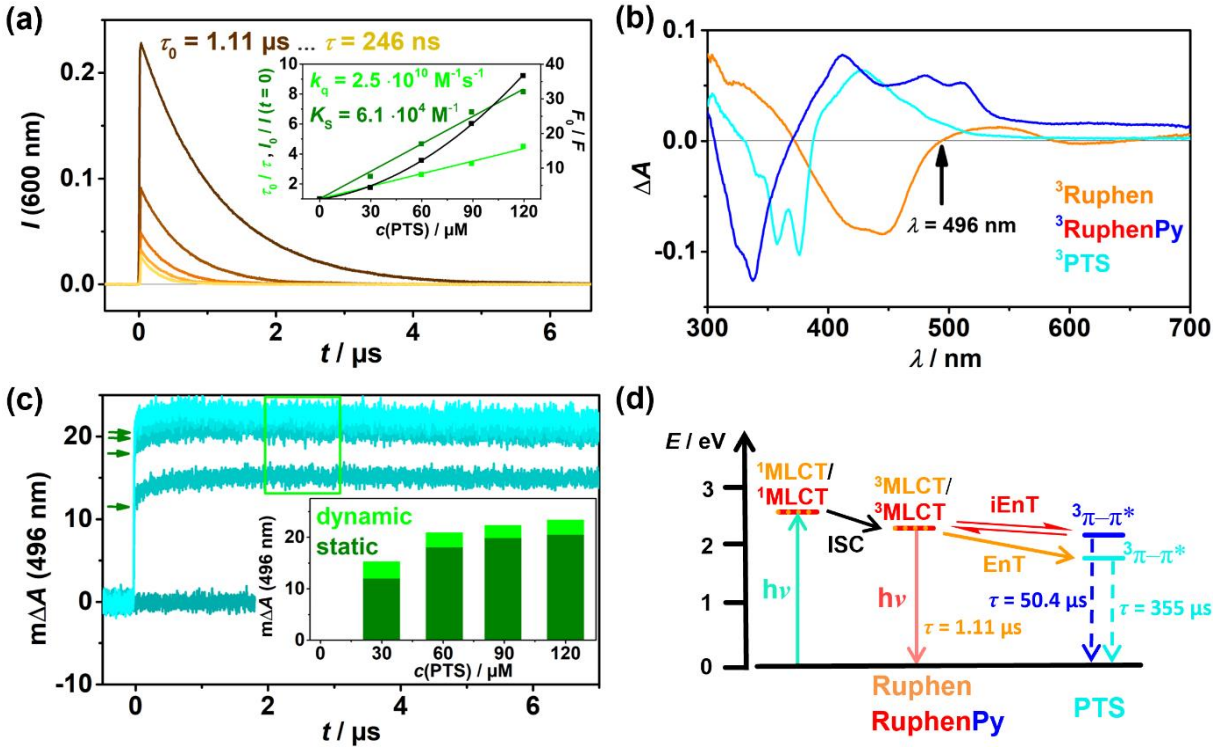

Figure 3 Coulomb-accelerated energy transfer. (a) Main plot: time-resolved emission traces of **Ruphen** (30 µM) with increasing **PTS** concentrations (30 µM steps) in Ar-saturated water with their corresponding lifetimes after laser excitation (λ = 532 nm, ~5 ns pulses, 50 mJ). Inset: Stern–Volmer-plots for static quenching (intensity *I* at *t* = 0 µs), dynamic quenching (τ) and total emission quenching (*F*). (b) Transient absorption spectra of ^{3}**Ruphen** (*c*(**Ruphen**) = 30 µM, orange, delay 50 ns), ^{3}**RuphenPy** (*c*(**RuphenPy**) = 30 µM, blue, delay 50 ns) and ^{3}**PTS** (*c*(**PTS**) = 30 µM, *c*(**Ruphen**) = 30 µM, cyan, delay 5 µs) after laser excitation (λ = 532 nm) in Ar-saturated water. (c) Main plot: time-resolved transient absorption traces of the same solutions as in (a) at λ_{det} = 496 nm with an indication of sub-ns static energy transfer (dark green arrows). Inset: **PTS** concentration-dependent total transient absorption signals at λ_{det} = 496 nm with respective contributions of static quenching (dark green arrows) and dynamic quenching (light green box). See text for further details. (d) Simplified energy diagram demonstrating the formation of long-lived organic triplet states in ruthenium complex-pyrene dyads.

Exploiting the Long ^{3}PTS Lifetime for Photooxygenations

For excited-state quenching to be efficient, the product of the quenching rate k_q, the natural lifetime τ of the excited state and the quencher concentration [Q] should be as high as possible. If τ is already very high, high quenching efficiencies are possible even with relatively small values of k_q or [Q]. This is demonstrated by the example of the quencher oxygen in air-saturated water, which is present in a very small concentration (0.27 mM O_2 in neat water at 25°C, see sections S.3.2 and S5.2.4 kinetic simulations)[95]. The relatively short natural triplet lifetime of **Ruphen**, 1.1 µs, leads to a maximum oxygen quenching efficiency η on the order of 50% under our conditions.[36] In contrast, the dyads, which are characterized by much longer triplet lifetimes, exhibit remarkable quenching efficiencies approaching quantitative values even when non-diffusion controlled quenching processes are considered. The experimentally measured quenching efficiencies in air-saturated water are shown in Figure 4.

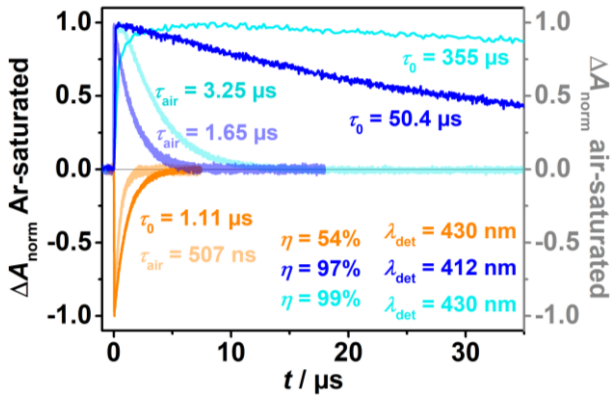

Figure 4 Normalized time-resolved transient absorption traces of the same solutions as in Figure 3 (b) in Ar- or air-saturated water with their corresponding lifetimes and calculated efficiencies for quenching by dissolved oxygen. Complete raw data sets for the long-lived triplets can be found in Figure S55.

Quenching the triplet states of **Ruphen** or pyrene derivatives through Dexter energy transfer with triplet oxygen results in the generation of singlet oxygen ($^1O_2$),[36] an impactful species for chemical synthesis, in medicine or the environment.[105–111] Due to the very short lifetime and the near-zero phosphorescence quantum yield of $^1O_2$ in water, it is difficult to detect and quantify this species spectroscopically.[112] However, there are multiple techniques available to confirm the presence of singlet oxygen in solution.[107] The RNO method, as developed by Kraljić and Mohsni,[113] offers a reliable and specific way of detecting $^1O_2$ in aqueous environments. Briefly, in this approach a nitrosyl compound (*N*,*N*-dimethyl-4-nitrosoaniline, RNO) undergoes oxidation to generate the corresponding nitro compound, which is facilitated by imidazole acting as a catalyst. The reduction in the RNO concentration can be quantified through UV-vis spectroscopy and is directly proportional to the rate of $^1O_2$ formation.

Consequently, this method enables a direct comparative analysis between the dyads regarding their $^1O_2$ production capabilities (see also section S3.1 of the SI). In a recent comparative study, we already investigated **Ruphen** and the molecular dyad **RuphenPy** employing the RNO method[36] and observed a threefold $^1O_2$ quantum yield increase for **RuphenPy**. This quantum yield increase is clearly more pronounced compared to what would be expected from the oxygen quenching efficiencies (Figure 4). This discrepancy is likely a result of the higher redox reactivity of ^{3}**Ruphen**[57,114] facilitating additional electron transfer quenching pathways with dissolved oxygen that are less favored for a purely pyrene localized triplet. Interestingly, the $^1O_2$ assay revealed that the Coulombic dyad possesses essentially the same $^1O_2$ formation efficiency as the molecular dyad **RuphenPy**, which is displayed in the inset in Figure 5 (b). These experiments further substantiate that the addition of a charge-adapted organic acceptor to an ionic metal complex sensitizer can lead to superior photochemical properties resembling those of more sophisticated dyads with covalent linkage of the two chromophores.

The outstanding ability of the Coulombic dyad to efficiently produce singlet oxygen in air-saturated water prompted us to perform photooxygenation reactions of the promising platform chemical 5-(hydroxymethyl)furan-2-carbaldehyde (**5-HMF**), which can be obtained from sugars.[115,116] The **5-HMF** photooxidation yields the potential polymer precursor 5-hydroxy-5-(hydroxymethyl)-furan-2(5H)-one,[36,117] and the valuable C_1 building block formic acid as a by-product in a 1:1 ratio. For a meaningful comparison with the molecular dyad, **PTS** was used for the Coulombic dyad at the same concentration as **Ruphen** (60 µM), resulting in 92% ^{3}**Ruphen** quenching even without a **PTS** excess. It was further shown that a catalyst loading of only 0.2 mol% of the Coulombic dyad gives suitable conversion rates for our comparative experiments, which is discussed in more detail in the SI (section S5.2.1). Using only **Ruphen** (see Figure 5 (a), left panel) at a substrate concentration of 30 mM, a yield of 61% (with the same conversion) is achieved after 5 h of 525 nm LED irradiation. Under identical conditions, the molecular dyad **RuphenPy** exhibits a higher initial product formation rate than **Ruphen**, but this advantage rapidly diminishes. After 5 h of irradiation, the molecular dyad reaches a yield of 58% at a substrate conversion of 65%. The initially increased product formation rate is consistent with previous $^1O_2$ assay results and is in line with expectations.[36] However, the lower performance of the molecular dyad under prolonged irradiation time may indicate a limited photostability of this tailor-made molecule. In welcome contrast, the Coulombic dyad maintains a high product formation rate such that the reaction approaches complete conversion after just 5 h, yielding a yield of 93% and a corresponding turnover number (TON) of 465. Control experiments conducted in the absence of light or any constituent of the catalytic system,

including oxygen, do not yield any product formation. For comparison, traditional organic photocatalysts for singlet oxygen generation, such as rose bengal, methylene blue, and eosin Y,[118–125] were employed in the experiments. However, their performance was notably lower, with yields below 20% following irradiation under our standardized conditions (yellow, pink and pale blue traces in Figure 5 (b)), despite their considerably higher extinction coefficients in the green spectral region compared to the employed ruthenium complexes. This discrepancy is attributed to the comparatively low (photo)stability of these organic photocatalysts.

Moreover, it was observed that the reaction rate in D_2O, where the lifetime of $^1O_2$ is about twenty times longer, is almost identical to that in H_2O (see SI, section S5.2.2).[126] This observation rules out the [2+2] cycloaddition between $^1O_2$ and **5-HMF** as the rate-determining step of the reaction. Alternatively, it seems plausible that the oxygen uptake rate in water serves as a limiting factor for the reaction rate. In this context, LFP was used to estimate the oxygen concentration during the ongoing reaction (see SI, section S5.2.3). An equilibrium oxygen concentration is assumed to be reached, which is primarily influenced by the uptake of oxygen from the atmosphere and its depletion as a result of the photoreaction. This analysis yields an "*in operando"* oxygen concentration of 0.16 mM for the use of the Coulombic dyad and 0.23 mM for **Ruphen**, which is in line with the observed faster conversion rate for the former. At an effective concentration of dissolved oxygen during irradiation as low as 0.16 mM, the quenching efficiency of ^{3}**PTS** still exceeds 90%. Thus, the Coulombic dyad maintains a high performance even at very low quencher concentrations.

Under conditions of much higher substrate concentration (0.33 M instead of 30 mM **5-HMF**), the Coulombic dyad shows an impressive TON of 3000 (Figure 5 (c)). Remarkably, by increasing the concentration of inexpensive **PTS** while keeping all other conditions identical, a TON of 5400 with respect to the ruthenium catalyst was reached, which represents a 4.2-fold increase compared to what was obtained with conventional **Ruphen**. The molecular dyad gives a slightly higher TON (1700) than **Ruphen**, indicating that dyad degradation (likely via $^1O_2$) is slower at very high substrate concentrations. Moreover, sunlight was used for sensitizer excitation (see SI, section S5.2.5). In this photoreaction, we observed a 2.4-fold increase in the reaction yield (84% vs 35%) when using the Coulombic dyad instead of **Ruphen**, demonstrating that the easy-to-use Coulombic dyad approach is also attractive for solar-driven applications.

A variety of products can be obtained starting from **5-HMF**.[116] When the photooxygenation process is carried out under alkaline conditions, it leads to *in situ* ring opening of 5-hydroxy-5-

(hydroxymethyl)-furan-2(5H)-one, forming (Z)-5-hydroxy-4-keto-2-pentenoic acid (see SI, section S5.2.7).[36] This product has direct potential as a monomeric building block for biopolymers. Interestingly, under alkaline conditions, the Coulombic dyad shows the same performance as under neutral-to-acidic conditions, which implies that the novel dyad approach can be exploited regardless of the pH value of the solution. All these results not only confirm the possibility to mimic the photophysical advantages of a molecular dyad by adding the oppositely charged pyrene **PTS** to **Ruphen** solutions, but they also highlight that achieving much higher reaction rates and TONs in practical applications are feasible by adding an inexpensive additive (**PTS**, less than 0.3 € per mmol[127] as sodium salt) to a precious photocatalyst (**Ruphen**, 32 € per mmol[127] as chloride salt).

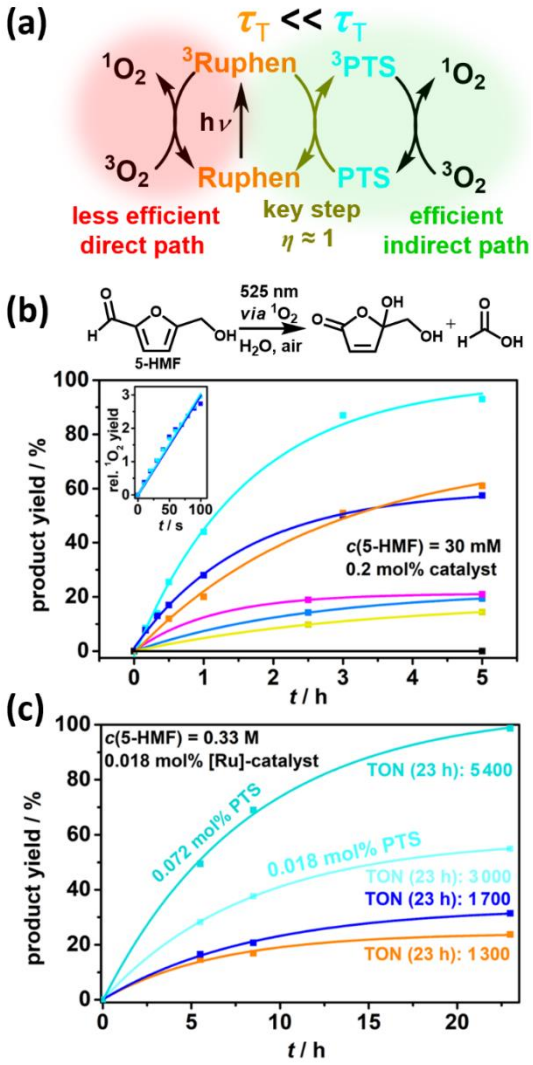

Figure 5 5-HMF photooxygenation in water. (a) Mechanism for conventional, less efficient (left) and improved, efficient (right) generation of singlet oxygen in air-saturated water and (b) reaction equation for the **5-HMF** test reaction. Main plot: time-resolved product yield (lactone) during irradiation experiments (LED with $\lambda_{max,exc}$ = 525 nm) with a solution of **5-HMF** (30 mM), 0.2 mol% catalyst (orange: **Ruphen**, blue: **RuphenPy**, cyan: **Ruphen** and **PTS**, magenta: rose bengal, pale blue: methylene blue, yellow: eosin Y, black: **PTS**) in air-saturated water at 20 °C. Inset: Relative singlet oxygen formation yields for the Coulombic and molecular dyad at the employed catalyst concentrations determined by the RNO method. (c) Product yields and the resulting TON after 23 h of irradiation with a higher substrate concentration (0.33 M).

Next, we extended our investigations to the synthesis of a sulfoxide in water. The sulfoxide moiety is a highly important group in organic and medical chemistry.[128] One elegant and selective way of forming this functional group from the respective thioether is the reaction with $^1O_2$.[129] We selected the photooxygenation of thioanisole (**TAN**) as a test reaction, which cannot be carried out in water at room temperature for solubility reasons,[130,131] but the limited water solubility of **TAN** can be addressed by increasing the temperature of the reaction mixture to 50 °C. The obtained product shows a better water solubility than **TAN** at room temperature and it can be quantified via ^{1}H NMR spectroscopy under the chosen conditions (see section S5.3).

Temperature variations lead to pronounced changes in the natural and oxygen-quenched lifetimes of triplet states, which consequently results in different oxygen quenching efficiencies. Complementary quenching studies at an elevated temperature of 50 °C revealed that the quenching efficiencies of ^{3}**PTS** and ^{3}**RuphenPy** by O_2 remain remarkably high at 99% and 90%, respectively. In contrast, the quenching efficiency of ^{3}**Ruphen** drops significantly to 43% (see SI, section S3.3). In the course of the photooxygenation of **TAN** (Figure 6), a flattening in the reaction progress curve is evident when **Ruphen** and **RuphenPy** are used as photocatalysts, indicating incomplete conversion most likely as a result of catalyst photodegradation. This phenomenon is most pronounced for **Ruphen** and related photoactive metal complexes, for which photodegradation is known to proceed in a thermally activated manner via a metal-centered excited state.[132–134] In stark contrast, the Coulombic dyad shows a yield exceeding 90% and no discernible signs of degradation within the system. We attribute this resistance to the rapid and quantitative quenching of ^{3}**Ruphen** by **PTS**, effectively preventing thermally activated degradation. The improved stability of the catalytic system at higher temperatures is also important for applications on larger scales, when heating can be a side effect of intense photoirradiation. The photooxygenation results at elevated temperatures thus revealed another advantage of Coulombic dyads over conventional metal complexes and molecular dyads.

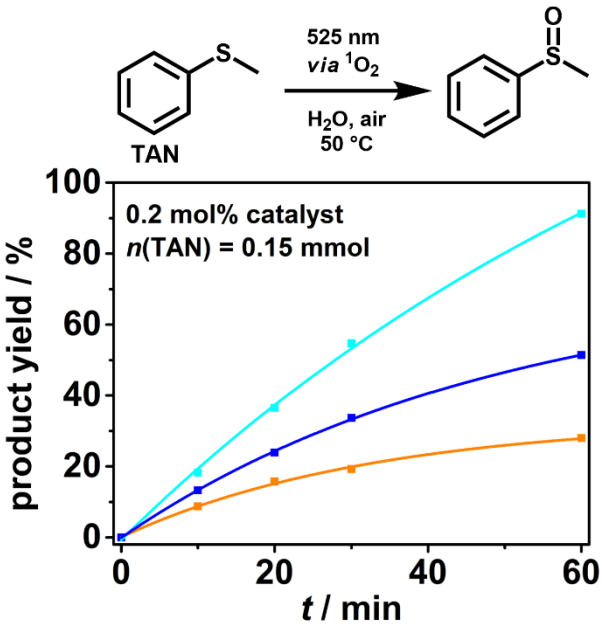

Figure 6 Time-resolved product yields for the formation of methyl phenyl sulfoxide from **TAN** (30 mM in total) with 0.2 mol% catalyst (orange: **Ruphen**, blue: **RuphenPy**, cyan: **Ruphen** and **PTS**) and LED irradiation ($\lambda_{max,exc}$ = 525 nm) in air-saturated water at 50 °C. See text for details.

Improving the Electron Transfer Reactivity with Coulombic Dyads

Building on the substantial improvements of the photooxygenation efficiencies described in the preceding section and encouraged by reports dealing with improved electron transfer photoreactivity of molecular dyads,[38,50–52] we explored whether the **Ruphen–PTS** pair is a superior catalyst for photoreductions. After excitation of the sensitizer **Ruphen**, the resulting ^{3}**MLCT** state can be reductively quenched by the ascorbate monoanion **HAsc**$^-$. This electron transfer quenching process yields **Ruphen**$^{\bullet-}$ and **HAsc**$^\bullet$ as a spin-correlated radical pair within the so-called solvent cage, which is born in the same spin state as the photoexcited precursor, *i.e.* in a triplet state.[38,135–137] Direct geminate recombination is spin-forbidden for a triplet pair, which can enable quantitative cage escape yielding the desired "free" radicals/radical ions that initiate photoreactions.[40,41,138,139] However, the high spin-orbit coupling caused by the heavy atom ruthenium induces radical-pair ISC, and the singlet pair so obtained undergoes highly efficient in-cage recombination. This mechanism is the reason for the frequently observed lousy cage escape quantum yields for photoinduced electron transfer reactions with 4d and 5d metal complexes.[38,42–44,140] In the case of the reductive quenching of **Ruphen** (see Figure 7 (a)) by **HAsc**$^-$, **Ruphen**$^{\bullet-}$[141,142] is produced with a cage escape quantum yield of 0.21 under our conditions (SI, section S8.2). This means that unproductive back electron transfer within the solvent cage dominates. The cage escape quantum yields were determined using the carefully calibrated absorption spectra of the respective species (see sections S7 and S8 for further explanations), which are displayed in Figure 7 (b). As we found, ^{3}**PTS** generated by sensitization with **Ruphen** with a nearly quantitative yield can also be effectively reduced by **HAsc**$^-$ in an aqueous environment, giving rise to **PTS**$^{\bullet-}$.[101,143] **PTS**$^{\bullet-}$ exhibits a characteristic absorption maximum at 510 nm with an extinction coefficient of 29000 $M^{-1}cm^{-1}$ (SI, section S7.5). An outstanding cage-escape quantum yield close to unity (within the experimental error) was determined for this process. In contrast to **Ruphen**, **PTS** lacks a comparable heavy atom, making the rate of radical-pair ISC negligible, thereby ensuring a maximized quantum yield for cage escape.

To test whether the divergent cage escape yields are accompanied by an improved photocatalytic reactivity of the Coulombic dyad, the reductive dehalogenation of 2-bromopyrazine (**2-BP**) was selected as the first benchmark reaction.[144] Under our standardized conditions, we used 10 mM **2-BP** and one equivalent of **NaHAsc**, which is a common electron donor in aqueous photocatalytic cycles.[103,145–148] The ascorbate monoanion is a reversible electron donor, ensuring that significant **HAsc**$^-$ decomposition does not occur, and the stable

ascorbyl radical undergoes disproportionation partially regenerating **HAsc**$^-$.[149] Hence, an **NaHAsc** excess is not required. Under these specific conditions and in the absence of **PTS**, the triplet state of pure **Ruphen** is reductively quenched with an efficiency of 0.84 (k_q = 4.5·10^8 M^{-1}s^{-1}, section S6.1). Taking the low cage-escape quantum yield of only 0.21 into account, a theoretical **Ruphen**$^{\bullet-}$ quantum yield of 0.18 is predicted, which is in close agreement with the measured total quantum yield of 0.16, as demonstrated in Figure 7 (d). In stark contrast, when the Coulombic dyad is used through the addition of **PTS**, the quenching of the ^{3}**Ruphen** occurs predominantly by an energy transfer to give ^{3}**PTS** because dynamic quenching by **HAsc**$^-$ cannot compete with static quenching by **PTS**. Although ^{3}**PTS** is reduced by **HAsc**$^-$ with a lower rate constant (k_q = 2.3·10^7 M^{-1}s^{-1}, section S6.2) than ^{3}**Ruphen**, quantitative quenching is possible owing to the much longer natural triplet lifetime of the organic chromophore. Combined with the high cage escape yield for this step, an overall quantum yield for the formation of **PTS**$^{\bullet-}$ as high as 0.97 (expected relative error below 20%) is achieved. No electron transfer from **PTS**$^{\bullet-}$ to the **Ruphen** ground state was observed, indicating that the reduction potential of **PTS**$^{\bullet-}$ is below that of **Ruphen**$^{\bullet-}$. The addition of high salt concentrations might attenuate the attractive interactions within the Coulombic dyad due to salt effects.[63,150] However, under our conditions with moderate salt concentrations (c(**NaHAsc**) = 10 mM), the static and dynamic quenching of ^{3}**Ruphen** by **PTS** is hardly affected such that **PTS**$^{\bullet-}$ quantum yields close to unity are within reach despite the seemingly complicated mechanism (Figure 7 (a)).

Next, the reactions between the radical ions **Ruphen**$^{\bullet-}$ or **PTS**$^{\bullet-}$ and the substrate **2-BP** were analyzed. After the **2-BP** reduction by one of those radicals, a very rapid cleavage of the halide and the formation of a pyrazine σ-radical is expected to occur,[144] which in turn abstracts an hydrogen atom from **HAsc**$^-$ or its oxidized products.[151] **Ruphen**$^{\bullet-}$ reacts with a rate constant of k_q ~ 3·10^9 M^{-1}s^{-1}, which corresponds to essentially complete quenching considering the **Ruphen**$^{\bullet-}$ lifetime of about 200 µs at a chosen concentration of c(**2-BP**) = 10 mM. In line with the lower redox potential, **PTS**$^{\bullet-}$ is slowly intercepted by **2-BP** at a rate of k_q ~ 4·10^5 M^{-1}s^{-1}. Taking its prolonged lifetime exceeding 800 µs, an efficiency of the **2-BP** activation by **PTS**$^{\bullet-}$ of 75% is calculated at the initial **2-BP** concentration (10 mM). When comparing the efficiencies of the individual steps in both catalytic cycles (Figure 7 (a)), the non-quantitative quenching of ^{3}**Ruphen** by **HAsc**$^-$ and the non-quantitative quenching of **PTS**$^{\bullet-}$ by **2-BP** almost cancel each other out, so that the performance of the two photoredox cycles is mainly determined by the cage escape efficiencies of the photoreduction steps. The time-resolved yields of the lab-scale reaction confirm the trend previously characterized through LFP measurements. In the presence of **Ruphen** only, the dehalogenation of **2-BP** is quite slow,

resulting in a yield of 16% after 3 h of irradiation. Gratifyingly, when utilizing the Coulombic dyad, a yield as high as 94% is achieved after the same irradiation duration (Figure 7 (c)). The slightly higher efficiency increase when using **PTS** (compared to what can be estimated from the LFP studies in MilliQ water) can be explained by the fact that D_2O was used as the solvent for the irradiation experiments, whereas the mechanistic studies were carried out in H_2O. This remarkable reaction quantum yield enhancement clearly demonstrates the advantages of a Coulombic dyad, which are simply achieved through the addition of an inexpensive additive.

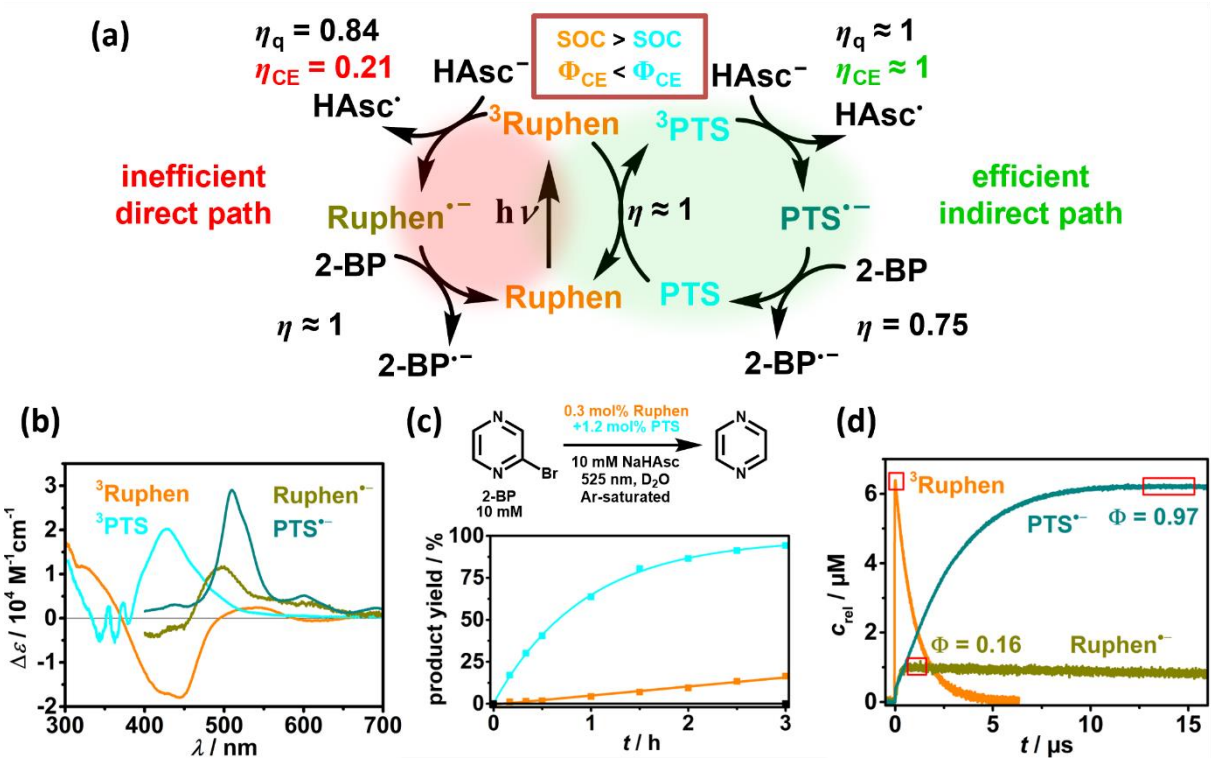

Figure 7 Efficient electron transfer reactions enabled by a Coulombic dyad. (a) Mechanism for inefficient (left) and efficient (right) reductive dehalogenation of **2-BP**. (b) Calibrated transient absorption spectra of ^{3}**Ruphen** (orange), ^{3}**PTS** (cyan), **Ruphen**$^{\bullet-}$ (ochre) and **PTS**$^{\bullet-}$ (petrol,) after laser excitation (532 nm) in Ar-saturated water. See SI for details regarding the spectral calibration. (c) Reaction equation with pertinent conditions and time-resolved product yield of the dehalogenation of **2-BP** (10 mM) with 0.3 mol% **Ruphen** (orange)/0.3 mol% **Ruphen** and 1.2 mol% **PTS** (cyan)/1.2 mol% **PTS** (black) upon LED irradiation ($\lambda_{max,exc}$ = 525 nm) in Ar-saturated water (D_2O) at 20 °C. (d) Transient absorption traces monitoring the concentrations of key species of solutions containing **Ruphen** (30 µM, λ_{det} = 455 nm, orange), **Ruphen** and **NaHAsc** (30 µM and 10 mM, respectively, λ_{det} = 496 nm, ocher), **Ruphen**, **PTS** and **NaHAsc** (30 µM, 120 µM and 10 mM, λ_{det} = 510 nm, petrol) after the laser pulse (λ_{exc} = 532 nm). Red boxes indicate the maximum TA values used for quantum yield determinations of **Ruphen**$^{\bullet-}$ or **PTS**$^{\bullet-}$ formation.

Finally, the Coulombic dyad was also employed for pinacol coupling reactions[152–154] of fluorinated benzaldehyde derivatives. The catalytic cycle of reductive substrate activation is the same as above for the **2-BP** dehalogenation,[103,155] and the electron transfer from **Ruphen**$^{\bullet-}$ or

PTS$^{\bullet-}$ to the model substrate 2-fluorobenzaldehyde (**2-FBA**) exhibits similar efficiency values (see SI, sections S6.5 and S6.6) approaching quantitative quenching. The exclusive presence of the pinacol product produced by dimerization of one-electron reduced substrate molecules is confirmed by both ^{1}H NMR and ^{19}F NMR analyses after the reaction. **Ruphen** irradiation in the presence of ascorbate led to yields ranging from 25% to 35% for the different derivatives, while the Coulombic dyad gave remarkable results ranging from 70% yield to quantitative conversion. In the context of pinacol coupling, a non-linear or even quadratic correlation between the overall reaction rate and the concentration of the **2-FBA** radical (anion) is expected. Based on our quantitative LFP measurements, reaction rates being faster by one order of magnitude could in principle result with the Coulombic dyad. However, the substantial but less pronounced difference in reaction rates, a factor of 3.3 within the first hour of photoirradiation (Figure 8 (b)), can be attributed to the slow decomposition of **PTS** in this particular example as confirmed by NMR experiments. Nevertheless, the catalyst decomposition products do not cause significant problems and the addition of inexpensive **PTS** clearly leads to a reactivity boost.

It is worth mentioning that successful transformations of practically water-insoluble benzaldehyde derivatives bearing a CF_3 group are feasible through the utilization of the promising food additive hydroxypropyl-*β*-cyclodextrin (**HPCD**), which seemingly does not interfere with the Coulombic dyad and the catalytic cycle. This cyclic sugar possesses the ability to encapsulate hydrophobic substances within its interior, thereby facilitating their solubilization in water.[155,156] A dynamic equilibrium exists between the encapsulated and “free” forms of the substrates in solution. The reaction of the aldehyde with the activated catalysts **Ruphen**$^{\bullet-}$ or **PTS**$^{\bullet-}$ likely occurs with the non-complexed substrate present in solution. The highly hydrophobic pinacol product is also encapsulated within **HPCD**, which avoids solubility issues throughout the photoreaction. Hence, the Coulombic dyad has been effectively employed for pinacol coupling reactions – even with water-insoluble carbonyl compounds – resulting in significantly enhanced reaction kinetics and a much more efficient use of the precious ruthenium sensitizer.

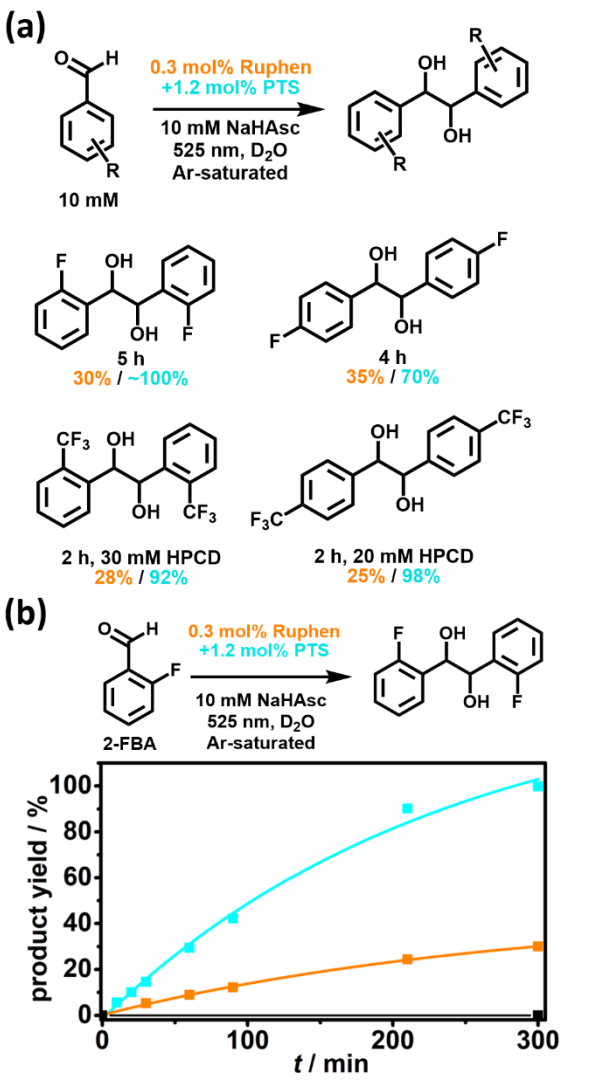

Figure 8 (a) Pinacol coupling of different benzaldehyde derivatives in neat D_2O or D_2O containing **HPCD**. (b) Time-resolved product yield of the pinacol coupling of **2-FBA** (10 mM) with 0.3 mol% **Ruphen** (orange)/0.3 mol% **Ruphen** and 1.2 mol% **PTS** (cyan)/1.2 mol% **PTS** (black) upon LED irradiation ($\lambda_{max,exc}$ = 525 nm) in Ar-saturated D_2O at 20 °C.

It seems natural to assume that a delicate balance between the solvent and both ionic chromophores is essential for realizing dyad properties without a covalent bond. In a recent study in which we focused on upconversion with $[Ru(phen)_3]^{2+}$ and the charge-adapted mediator pyrene-1-sulfonate (**PMS**), we did not observe static (*i.e.* dyad-like) energy transfer in DMF, neither upon mixing commercially available salts nor by using the synthesized salt $[Ru(phen)_3](\mathbf{PMS})_2$ lacking non-chromophoric counterions.[63] However, when dichloromethane is used as the solvent, that $[Ru(phen)_3](\mathbf{PMS})_2$ salt undergoes highly efficient static formation of long-lived ^{3}**PMS** upon selective excitation of the ruthenium unit in the visible (see SI, section S9.2). These findings unambiguously establish that Coulombic dyads are more than a lab curiosity in aqueous solutions. To demonstrate that the Coulombic dyad concept is not limited to ruthenium sensitizers in combination with pyrene derivatives, initial investigations with a

dicationic osmium sensitizer were carried out. Highly efficient and predominantly static energy transfer quenching was observed with $[Os(phen)_3]^{2+}$ and the anionic triplet energy-matched perylene-3,4,9,10-tetracarboxylate (section S9.1 of the SI). An impressive energy transfer reactivity improvement by as much as a factor of 15 was observed for this Coulombic dyad compared to $[Os(phen)_3]^{2+}$ alone (SI, Figure S49), which we attribute to the even shorter unquenched lifetime of the photoexcited metal complex in this case. Considering that numerous photoactive metal complexes are cationic in nature, the experiments of this section illustrate the potential of Coulombic dyads for versatile photochemical applications in different solvents.

Conclusions

In summary, we have demonstrated that efficient inorganic-organic hybrid photocatalysts with photochemical properties reminiscent of tailor-made bichromophores are formed simply by mixing commercially available salts in aqueous solution. As a result of Coulombic attraction, the organic triplet is produced with efficiencies close to unity upon visible-light excitation of a photoactive metal complex and a subsequent Dexter-type energy transfer. Compared to the triplet-excited metal complex, the organic triplet so obtained undergoes highly efficient energy and electron transfer key reaction steps owing to its longer lifetime and inherently more efficient cage escape yields. Both lab-scale irradiation experiments and detailed spectroscopic investigations highlight the beneficial properties of Coulombic dyads as easy-to-prepare catalysts with improved reaction quantum yields. Initial studies with other chromophore combinations and in other solvents imply that Coulombic dyads can be developed into a versatile catalyst class for efficient applications in the greater context of photochemical energy conversion.

Author contributions

M.S. performed the experimental work and designed most of the photochemical studies for the energy transfer catalysis chapter. M.S. and M.-S.B. shared the work for the mechanistic studies on the photoredox catalysis chapter and the corresponding irradiation experiments. A.C.S. and F.G. provided RuphenPy and $[Ru(phen)_3](PMS)_2$, respectively. M.S. performed the DFT calculations. C.K. conceived the project and provided guidance throughout the study. C.K. and M.S. wrote the initial draft of the manuscript. M.S. prepared the initial version of the SI. All authors contributed to the editing of the manuscript and the SI.

Supporting Information

The Supporting Information document contains:

Experimental details, additional spectroscopic results, raw data sets, quantum-mechanical calculations and details about the irradiation experiments.

Data Availability

All experimental data have been provided in the main text and the SI. The data sets shown in the main paper and DFT output files will be uploaded via the JGU library "Gutenberg Open Science" after acceptance of the manuscript.

Notes

The authors declare no competing financial interest.

Acknowledgements

We acknowledge generous financial support from the JGU Mainz and the German Research Foundation (DFG, grant number KE 2313/7-1). M.S. is grateful to the Chemical Industry Funds for a Kekulé fellowship. We thank David Pauly for carrying out first experiments with **PTS** in combination with sodium ascorbate. We thank Ernesto Llamas from Sketching-Science for drawing and allowing us to use the chemist displayed in the table of contents graphic. DTF calculations were conducted using the supercomputer Elwetritsch and advisory services offered by the University of Kaiserslautern-Landau (https://hpc.rz.rptu.de), which is a member of the AHRP and the Gauss Alliance e. V.

References

(1) Shaw, M. H.; Twilton, J.; MacMillan, D. W. C. Photoredox Catalysis in Organic Chemistry. *J. Org. Chem.* **2016**, *81* (16), 6898–6926. https://doi.org/10.1021/acs.joc.6b01449.

(2) Arias-Rotondo, D. M.; McCusker, J. K. The Photophysics of Photoredox Catalysis: A Roadmap for Catalyst Design. *Chem. Soc. Rev.* **2016**, *45* (21), 5803–5820. https://doi.org/10.1039/C6CS00526H.

(3) Romero, N. A.; Nicewicz, D. A. Organic Photoredox Catalysis. *Chem. Rev.* **2016**, *116* (17), 10075–10166. https://doi.org/10.1021/acs.chemrev.6b00057.

(4) Narayanam, J. M. R.; Stephenson, C. R. J. Visible Light Photoredox Catalysis: Applications in Organic Synthesis. *Chem. Soc. Rev.* **2011**, *40* (1), 102–113. https://doi.org/10.1039/B913880N.

(5) Großkopf, J.; Kratz, T.; Rigotti, T.; Bach, T. Enantioselective Photochemical Reactions Enabled by Triplet Energy Transfer. *Chem. Rev.* **2022**, *122* (2), 1626–1653. https://doi.org/10.1021/acs.chemrev.1c00272.
(6) Dutta, S.; Erchinger, J. E.; Strieth-Kalthoff, F.; Kleinmans, R.; Glorius, F. Energy Transfer Photocatalysis: Exciting Modes of Reactivity. *Chem. Soc. Rev.* **2024**, *53* (3), 1068–1089. https://doi.org/10.1039/D3CS00190C.
(7) Neveselý, T.; Wienhold, M.; Molloy, J. J.; Gilmour, R. Advances in the *E* → *Z* Isomerization of Alkenes Using Small Molecule Photocatalysts. *Chem. Rev.* **2022**, *122* (2), 2650–2694. https://doi.org/10.1021/acs.chemrev.1c00324.
(8) Noël, T.; Zysman-Colman, E. The Promise and Pitfalls of Photocatalysis for Organic Synthesis. *Chem Catal.* **2022**, *2* (3), 468–476. https://doi.org/10.1016/j.checat.2021.12.015.
(9) Crisenza, G. E. M.; Melchiorre, P. Chemistry Glows Green with Photoredox Catalysis. *Nat. Commun.* **2020**, *11* (1), 803. https://doi.org/10.1038/s41467-019-13887-8.
(10) Ravetz, B. D.; Pun, A. B.; Churchill, E. M.; Congreve, D. N.; Rovis, T.; Campos, L. M. Photoredox Catalysis Using Infrared Light via Triplet Fusion Upconversion. *Nature* **2019**, *565* (7739), 343–346. https://doi.org/10.1038/s41586-018-0835-2.
(11) MacKenzie, I. A.; Wang, L.; Onuska, N. P. R.; Williams, O. F.; Begam, K.; Moran, A. M.; Dunietz, B. D.; Nicewicz, D. A. Discovery and Characterization of an Acridine Radical Photoreductant. *Nature* **2020**, *580* (7801), 76–80. https://doi.org/10.1038/s41586-020-2131-1.
(12) Glaser, F.; Kerzig, C.; Wenger, O. S. Multi-Photon Excitation in Photoredox Catalysis: Concepts, Applications, Methods. *Angew. Chem. Int. Ed.* **2020**, *59* (26), 10266–10284. https://doi.org/10.1002/anie.201915762.
(13) Schreier, M. R.; Guo, X.; Pfund, B.; Okamoto, Y.; Ward, T. R.; Kerzig, C.; Wenger, O. S. Water-Soluble Tris(Cyclometalated) Iridium(III) Complexes for Aqueous Electron and Energy Transfer Photochemistry. *Acc. Chem. Res.* **2022**, *55* (9), 1290–1300. https://doi.org/10.1002/ejic.201900453.
(14) Marzo, L.; Pagire, S. K.; Reiser, O.; König, B. Visible-Light Photocatalysis: Does It Make a Difference in Organic Synthesis? *Angew. Chem. Int. Ed.* **2018**, *57* (32), 10034–10072. https://doi.org/10.1002/anie.201709766.
(15) Barham, J. P.; König, B. Synthetic Photoelectrochemistry. *Angew. Chem. Int. Ed.* **2020**, *59* (29), 11732–11747. https://doi.org/10.1002/anie.201913767.
(16) Ravetz, B. D.; Tay, N. E. S.; Joe, C. L.; Sezen-Edmonds, M.; Schmidt, M. A.; Tan, Y.; Janey, J. M.; Eastgate, M. D.; Rovis, T. Development of a Platform for Near-Infrared Photoredox Catalysis. *ACS Cent. Sci.* **2020**, *6* (11), 2053–2059. https://doi.org/10.1021/acscentsci.0c00948.
(17) Ziegenbalg, D.; Pannwitz, A.; Rau, S.; Dietzek-Ivanšić, B.; Streb, C. Comparative Evaluation of Light-Driven Catalysis: A Framework for Standardized Reporting of Data**. *Angew. Chem. Int. Ed.* **2022**, *61* (28), e202114106. https://doi.org/10.1002/anie.202114106.
(18) Cambié, D.; Bottecchia, C.; Straathof, N. J. W.; Hessel, V.; Noël, T. Applications of Continuous-Flow Photochemistry in Organic Synthesis, Material Science, and Water Treatment. *Chem. Rev.* **2016**, *116* (17), 10276–10341. https://doi.org/10.1021/acs.chemrev.5b00707.
(19) Speckmeier, E.; Fischer, T. G.; Zeitler, K. A Toolbox Approach To Construct Broadly Applicable Metal-Free Catalysts for Photoredox Chemistry: Deliberate Tuning of Redox Potentials and Importance of Halogens in Donor–Acceptor Cyanoarenes. *J. Am. Chem. Soc.* **2018**, *140* (45), 15353–15365. https://doi.org/10.1021/jacs.8b08933.
(20) Wenger, O. S. Photoactive Complexes with Earth-Abundant Metals. *J. Am. Chem. Soc.* **2018**, *140* (42), 13522–13533. https://doi.org/10.1021/jacs.8b08822.
(21) Kitzmann, W. R.; Heinze, K. Charge-Transfer and Spin-Flip States: Thriving as Complements. *Angew. Chem. Int. Ed.* **2023**, *62* (15), e202213207. https://doi.org/10.1002/anie.202213207.
(22) Zhang, Y.; Lee, T. S.; Favale, J. M.; Leary, D. C.; Petersen, J. L.; Scholes, G. D.; Castellano, F. N.; Milsmann, C. Delayed Fluorescence from a Zirconium(IV) Photosensitizer with Ligand-to-Metal Charge-Transfer Excited States. *Nat. Chem.* **2020**, *12* (4), 345–352. https://doi.org/10.1038/s41557-020-0430-7.
(23) Bryden, M. A.; Zysman-Colman, E. Organic Thermally Activated Delayed Fluorescence (TADF) Compounds Used in Photocatalysis. *Chem. Soc. Rev.* **2021**, *50* (13), 7587–7680. https://doi.org/10.1039/D1CS00198A.

(24) Chan, A. Y.; Ghosh, A.; Yarranton, J. T.; Twilton, J.; Jin, J.; Arias-Rotondo, D. M.; Sakai, H. A.; McCusker, J. K.; MacMillan, D. W. C. Exploiting the Marcus Inverted Region for First-Row Transition Metal–Based Photoredox Catalysis. *Science* **2023**, *382* (6667), 191–197. https://doi.org/10.1126/science.adj0612.
(25) De Groot, L. H. M.; Ilic, A.; Schwarz, J.; Wärnmark, K. Iron Photoredox Catalysis–Past, Present, and Future. *J. Am. Chem. Soc.* **2023**, *145* (17), 9369–9388. https://doi.org/10.1021/jacs.3c01000.
(26) Kim, D.; Dang, V. Q.; Teets, T. S. Improved Transition Metal Photosensitizers to Drive Advances in Photocatalysis. *Chem. Sci.* **2024**, *15* (1), 77–94. https://doi.org/10.1039/D3SC04580C.
(27) Swierk, J. R. The Cost of Quantum Yield. *Org. Process Res. Dev.* **2023**, *27* (7), 1411–1419. https://doi.org/10.1021/acs.oprd.3c00167.
(28) Buzzetti, L.; Crisenza, G. E. M.; Melchiorre, P. Mechanistic Studies in Photocatalysis. *Angew. Chem. Int. Ed.* **2019**, *58* (12), 3730–3747. https://doi.org/10.1002/anie.201809984.
(29) Wang, C.; Malinoski, A. Perspective: Mechanistic Investigations of Photocatalytic Processes with Time-Resolved Optical Spectroscopy. *J. Chem. Phys.* **2022**, *157* (16), 160901. https://doi.org/10.1063/5.0111162.
(30) Marchini, M.; Bergamini, G.; Cozzi, P. G.; Ceroni, P.; Balzani, V. Photoredox Catalysis: The Need to Elucidate the Photochemical Mechanism. *Angew. Chem. Int. Ed.* **2017**, *56* (42), 12820–12821. https://doi.org/10.1002/anie.201706217.
(31) De Kreijger, S.; Gillard, M.; Elias, B.; Troian-Gautier, L. Spectroscopic Techniques to Unravel Mechanistic Details in Light-Induced Transformations and Photoredox Catalysis. *ChemCatChem* **2024**, *16* (1), e202301100. https://doi.org/10.1002/cctc.202301100.
(32) Talbott, E. D.; Burnett, N. L.; Swierk, J. R. Mechanistic and Kinetic Studies of Visible Light Photoredox Reactions. *Chem. Phys. Rev.* **2023**, *4* (3), 031312. https://doi.org/10.1063/5.0156850.
(33) Koike, T.; Akita, M. Visible-Light Radical Reaction Designed by Ru- and Ir-Based Photoredox Catalysis. *Inorg. Chem. Front.* **2014**, *1* (8), 562–576. https://doi.org/10.1039/C4QI00053F.
(34) Teegardin, K.; Day, J. I.; Chan, J.; Weaver, J. Advances in Photocatalysis: A Microreview of Visible Light Mediated Ruthenium and Iridium Catalyzed Organic Transformations. *Org. Process Res. Dev.* **2016**, *20* (7), 1156–1163. https://doi.org/10.1021/acs.oprd.6b00101.
(35) Goldschmid, S. L.; Bednářová, E.; Beck, L. R.; Xie, K.; Tay, N. E. S.; Ravetz, B. D.; Li, J.; Joe, C. L.; Rovis, T. Tuning the Electrochemical and Photophysical Properties of Osmium-Based Photoredox Catalysts. *Synlett* **2022**, *33* (03), 247–258. https://doi.org/10.1055/s-0041-1737792.
(36) Sell, A. C.; Wetzel, J. C.; Schmitz, M.; Maijenburg, A. W.; Woltersdorf, G.; Naumann, R.; Kerzig, C. Water-Soluble Ruthenium Complex-Pyrene Dyads with Extended Triplet Lifetimes for Efficient Energy Transfer Applications. *Dalton Trans.* **2022**, *51* (28), 10799–10808. https://doi.org/10.1039/D2DT01157C.
(37) Wehlin, S. A. M.; Troian-Gautier, L.; Maurer, A. B.; Brennaman, M. K.; Meyer, G. J. Photophysical Characterization of New Osmium (II) Photocatalysts for Hydrohalic Acid Splitting. *J. Chem. Phys.* **2020**, *153* (5), 054307. https://doi.org/10.1063/5.0014269.
(38) Neumann, S.; Wenger, O. S.; Kerzig, C. Controlling Spin-Correlated Radical Pairs with Donor–Acceptor Dyads: A New Concept to Generate Reduced Metal Complexes for More Efficient Photocatalysis. *Chem. – Eur. J.* **2021**, *27* (12), 4115–4123. https://doi.org/10.1002/chem.202004638.
(39) Sittel, S.; Sell, A. C.; Hofmann, K.; Wiedemann, C.; Nau, J. P.; Kerzig, C.; Manolikakes, G.; Heinze, K. Visible-Light Induced Fixation of SO_2 into Organic Molecules with Polypyridine Chromium(III) Complexes. *ChemCatChem* **2023**, *15* (6), e202201562. https://doi.org/10.1002/cctc.202201562.
(40) Bürgin, T. H.; Glaser, F.; Wenger, O. S. Shedding Light on the Oxidizing Properties of Spin-Flip Excited States in a Cr^{III} Polypyridine Complex and Their Use in Photoredox Catalysis. *J. Am. Chem. Soc.* **2022**, *144* (31), 14181–14194. https://doi.org/10.1021/jacs.2c04465.
(41) Ripak, A.; De Kreijger, S.; Sampaio, R. N.; Vincent, C. A.; Cauët, É.; Jabin, I.; Tambar, U. K.; Elias, B.; Troian-Gautier, L. Photosensitized Activation of Diazonium Derivatives for C–B Bond Formation. *Chem Catal.* **2023**, *3* (2), 100490. https://doi.org/10.1016/j.checat.2022.100490.

(42) Ozawa, K.; Tamaki, Y.; Kamogawa, K.; Koike, K.; Ishitani, O. Factors Determining Formation Efficiencies of One-Electron-Reduced Species of Redox Photosensitizers. *J. Chem. Phys.* **2020**, *153* (15), 154302. https://doi.org/10.1063/5.0023593.
(43) Miedlar, K.; Das, P. K. Tris(2,2'-Bipyridine)Ruthenium(II)-Sensitized Photooxidation of Phenols. Environmental Effects on Electron Transfer Yields and Kinetics. *J. Am. Chem. Soc.* **1982**, *104* (26), 7462–7469. https://doi.org/10.1021/ja00390a012.
(44) Adams, R. E.; Schmehl, R. H. Micellar Effects on Photoinduced Electron Transfer in Aqueous Solutions Revisited: Dramatic Enhancement of Cage Escape Yields in Surfactant Ru(II) Diimine Complex/$[Ru(NH_3)_6]^{2+}$ Systems. *Langmuir* **2016**, *32* (34), 8598–8607. https://doi.org/10.1021/acs.langmuir.6b02193.
(45) Castellano, F. N. Altering Molecular Photophysics by Merging Organic and Inorganic Chromophores. *Acc. Chem. Res.* **2015**, *48* (3), 828–839. https://doi.org/10.1021/ar500385e.
(46) Castellano, F. N. Transition Metal Complexes Meet the Rylenes. *Dalton Trans.* **2012**, *41* (28), 8493. https://doi.org/10.1039/c2dt30765k.
(47) Howarth, A. J.; Majewski, M. B.; Wolf, M. O. Photophysical Properties and Applications of Coordination Complexes Incorporating Pyrene. *Coord. Chem. Rev.* **2015**, *282–283*, 139–149. https://doi.org/10.1016/j.ccr.2014.03.024.
(48) Schmid, M.; Brückmann, J.; Bösking, J.; Nauroozi, D.; Karnahl, M.; Rau, S.; Tschierlei, S. Merging of a Perylene Moiety Enables a Ru^{II} Photosensitizer with Long-Lived Excited States and the Efficient Production of Singlet Oxygen. *Chem. – Eur. J.* **2022**, *28*, e202103609. https://doi.org/10.1002/chem.202103609.
(49) Kerzig, C.; Wenger, O. S. Sensitized Triplet–Triplet Annihilation Upconversion in Water and Its Application to Photochemical Transformations. *Chem. Sci.* **2018**, *9* (32), 6670–6678. https://doi.org/10.1039/C8SC01829D.
(50) Wilson, G. J.; Launikonis, A.; Sasse, W. H. F.; Mau, A. W.-H. Chromophore-Specific Quenching of Ruthenium Trisbipyridine−Arene Bichromophores by Methyl Viologen. *J. Phys. Chem. A* **1998**, *102* (26), 5150–5156. https://doi.org/10.1021/jp973248s.
(51) Weinheimer, C.; Choi, Y.; Caldwell, T.; Gresham, P.; Olmsted, J. Effect of a Steric Spacer on Chromophoric Interactions of Ruthenium Complexes Containing Covalently Bound Anthracene. *J. Photochem. Photobiol. Chem.* **1994**, *78* (2), 119–126. https://doi.org/10.1016/1010-6030(93)03723-T.
(52) Ma, L.; Wang, P.; Wang, J.-Z.; Guo, S.; Zhang, Z.-M.; Zeng, X.-S.; Lu, T.-B. Bidirectional Sensitization in Ruthenium(II)-Antenna Dyad beyond Energy Flow of Biological Model for Efficient Photosynthesis. *Dyes Pigments* **2021**, *196*, 109811. https://doi.org/10.1016/j.dyepig.2021.109811.
(53) Guo, S.; Chen, K.-K.; Dong, R.; Zhang, Z.-M.; Zhao, J.; Lu, T.-B. Robust and Long-Lived Excited State Ru(II) Polyimine Photosensitizers Boost Hydrogen Production. *ACS Catal.* **2018**, *8* (9), 8659–8670. https://doi.org/10.1021/acscatal.8b02226.
(54) Deng, F.; Lazorski, M. S.; Castellano, F. N. Photon Upconversion Sensitized by a Ru(II)-Pyrenyl Chromophore. *Philos. Trans. R. Soc. Math. Phys. Eng. Sci.* **2015**, *373* (2044), 20140322. https://doi.org/10.1098/rsta.2014.0322.
(55) Lu, Y.; Wang, J.; McGoldrick, N.; Cui, X.; Zhao, J.; Caverly, C.; Twamley, B.; Ó Máille, G. M.; Irwin, B.; Conway-Kenny, R.; Draper, S. M. Iridium(III) Complexes Bearing Pyrene-Functionalized 1,10-Phenanthroline Ligands as Highly Efficient Sensitizers for Triplet-Triplet Annihilation Upconversion. *Angew. Chem. Int. Ed.* **2016**, *55* (47), 14688–14692. https://doi.org/10.1002/anie.201608442.
(56) Wang, P.; Guo, S.; Wang, H.-J.; Chen, K.-K.; Zhang, N.; Zhang, Z.-M.; Lu, T.-B. A Broadband and Strong Visible-Light-Absorbing Photosensitizer Boosts Hydrogen Evolution. *Nat. Commun.* **2019**, *10* (1), 3155. https://doi.org/10.1038/s41467-019-11099-8.
(57) Bertrams, M.-S.; Hermainski, K.; Mörsdorf, J.-M.; Ballmann, J.; Kerzig, C. Triplet Quenching Pathway Control with Molecular Dyads Enables the Identification of a Highly Oxidizing Annihilator Class. *Chem. Sci.* **2023**, *14* (32), 8583–8591. https://doi.org/10.1039/D3SC01725G.
(58) Potocny, A. M.; Phelan, B. T.; Sprague-Klein, E. A.; Mara, M. W.; Tiede, D. M.; Chen, L. X.; Mulfort, K. L. Harnessing Intermolecular Interactions to Promote Long-Lived Photoinduced Charge Separation from Copper Phenanthroline Chromophores. *Inorg. Chem.* **2022**, *61* (48), 19119–19133. https://doi.org/10.1021/acs.inorgchem.2c02648.

(59) Tsuji, Y.; Yamamoto, K.; Yamauchi, K.; Sakai, K. Near-Infrared Light-Driven Hydrogen Evolution from Water Using a Polypyridyl Triruthenium Photosensitizer. *Angew. Chem. Int. Ed.* **2018**, *57* (1), 208–212. https://doi.org/10.1002/anie.201708996.
(60) Li, G.; Swords, W. B.; Meyer, G. J. Bromide Photo-Oxidation Sensitized to Visible Light in Consecutive Ion Pairs. *J. Am. Chem. Soc.* **2017**, *139* (42), 14983–14991. https://doi.org/10.1021/jacs.7b06735.
(61) Deetz, A. M.; Goodwin, M. J.; Kober, E. A.; Meyer, G. J. Nanosecond Intra-Ionic Chloride Photo-Oxidation. *Inorg. Chem.* **2023**, *62* (29), 11414–11425. https://doi.org/10.1021/acs.inorgchem.3c00970.
(62) Freys, J. C.; Wenger, O. S. Supramolecular and Intramolecular Energy Transfer with Ruthenium-Anthracene Donor-Acceptor Couples: Salt Bridge versus Covalent Bond. *Eur. J. Inorg. Chem.* **2010**, *2010* (35), 5509–5516. https://doi.org/10.1002/ejic.201000815.
(63) Glaser, F.; Schmitz, M.; Kerzig, C. Coulomb Interactions for Mediator-Enhanced Sensitized Triplet–Triplet Annihilation Upconversion in Solution. *Nanoscale* **2024**, *16* (1), 123–137. https://doi.org/10.1039/D3NR05265F.
(64) Balzani, V.; Sabbatini, N.; Scandola, F. "Second-Sphere" Photochemistry and Photophysics of Coordination Compounds. *Chem. Rev.* **1986**, *86* (2), 319–337. https://doi.org/10.1021/cr00072a002.
(65) Vogler, A.; Kunkely, H. Photochemistry of Transition Metal Complexes Induced by Outer-Sphere Charge Transfer Excitation. In *Photoinduced Electron Transfer II*; Mattay, J., Ed.; Dewar, M. J. S., Dunitz, J. D., Hafner, K., Itô, S., Lehn, J.-M., Niedenzu, K., Raymond, K. N., Rees, C. W., Vögtle, F., Series Eds.; Topics in Current Chemistry; Springer Berlin Heidelberg: Berlin, Heidelberg, 1990; Vol. 158, pp 1–30. https://doi.org/10.1007/3-540-52568-8_1.
(66) Billing, R. Optical and Photoinduced Electron Transfer in Ion Pairs of Coordination Compounds. *Coord. Chem. Rev.* **1997**, *159*, 257–270. https://doi.org/10.1016/S0010-8545(96)01288-X.
(67) Knighton, R. C.; Beames, J. M.; Pope, S. J. A. Polycationic Ru(II) Luminophores: Syntheses, Photophysics, and Application in Electrostatically Driven Sensitization of Lanthanide Luminescence. *Inorg. Chem.* **2023**, *62* (48), 19446–19456. https://doi.org/10.1021/acs.inorgchem.3c02352.
(68) Uraguchi, D.; Kimura, Y.; Ueoka, F.; Ooi, T. Urea as a Redox-Active Directing Group under Asymmetric Photocatalysis of Iridium-Chiral Borate Ion Pairs. *J. Am. Chem. Soc.* **2020**, *142* (46), 19462–19467. https://doi.org/10.1021/jacs.0c09468.
(69) Guerrero, I.; Viñas, C.; Fontrodona, X.; Romero, I.; Teixidor, F. Aqueous Persistent Noncovalent Ion-Pair Cooperative Coupling in a Ruthenium Cobaltabis(Dicarbollide) System as a Highly Efficient Photoredox Oxidation Catalyst. *Inorg. Chem.* **2021**, *60* (12), 8898–8907. https://doi.org/10.1021/acs.inorgchem.1c00751.
(70) Farney, E. P.; Chapman, S. J.; Swords, W. B.; Torelli, M. D.; Hamers, R. J.; Yoon, T. P. Discovery and Elucidation of Counteranion Dependence in Photoredox Catalysis. *J. Am. Chem. Soc.* **2019**, *141* (15), 6385–6391. https://doi.org/10.1021/jacs.9b01885.
(71) Sau, S. C.; Schmitz, M.; Burdenski, C.; Baumert, M.; Antoni, P. W.; Kerzig, C.; Hansmann, M. M. Dicationic Acridinium/Carbene Hybrids as Strongly Oxidizing Photocatalysts. *J. Am. Chem. Soc.* **2024**,*146* (5), 3416–3426. https://doi.org/10.1021/jacs.3c12766.
(72) Earley, J. D.; Zieleniewska, A.; Ripberger, H. H.; Shin, N. Y.; Lazorski, M. S.; Mast, Z. J.; Sayre, H. J.; McCusker, J. K.; Scholes, G. D.; Knowles, R. R.; Reid, O. G.; Rumbles, G. Ion-Pair Reorganization Regulates Reactivity in Photoredox Catalysts. *Nat. Chem.* **2022**, *14* (7), 746–753. https://doi.org/10.1038/s41557-022-00911-6.
(73) Das, S.; Zhu, C.; Demirbas, D.; Bill, E.; De, C. K.; List, B. Asymmetric Counteranion-Directed Photoredox Catalysis. *Science* **2023**, *379* (6631), 494–499. https://doi.org/10.1126/science.ade8190.
(74) Ohmura, S.; Katagiri, K.; Kato, H.; Horibe, T.; Miyakawa, S.; Hasegawa, J.; Ishihara, K. Highly Enantioselective Radical Cation [2 + 2] and [4 + 2] Cycloadditions by Chiral Iron(III) Photoredox Catalysis. *J. Am. Chem. Soc.* **2023**, *145* (28), 15054–15060. https://doi.org/10.1021/jacs.3c04010.
(75) Takizawa, S.; Okuyama, T.; Yamazaki, S.; Sato, K.; Masai, H.; Iwai, T.; Murata, S.; Terao, J. Ion Pairing of Cationic and Anionic Ir(III) Photosensitizers for Photocatalytic CO_2 Reduction at

Lipid–Membrane Surfaces. *J. Am. Chem. Soc.* **2023**, *145* (28), 15049–15053. https://doi.org/10.1021/jacs.3c03625.
(76) Schulte, A. M.; Alachouzos, G.; Szymanski, W.; Feringa, B. L. The Fate of the Contact Ion Pair Determines the Photochemistry of Coumarin-Based Photocleavable Protecting Groups. *Chem. Sci.* **2024**, 10.1039.D3SC05725A. https://doi.org/10.1039/D3SC05725A.
(77) Schirmer, T. E.; König, B. Ion-Pairing Catalysis in Stereoselective, Light-Induced Transformations. *J. Am. Chem. Soc.* **2022**, *144* (42), 19207–19218. https://doi.org/10.1021/jacs.2c04759.
(78) Morack, T.; Mück-Lichtenfeld, C.; Gilmour, R. Bioinspired Radical Stetter Reaction: Radical Umpolung Enabled by Ion-Pair Photocatalysis. *Angew. Chem. Int. Ed.* **2019**, *58* (4), 1208–1212. https://doi.org/10.1002/anie.201809601.
(79) Herr, P.; Kerzig, C.; Larsen, C. B.; Häussinger, D.; Wenger, O. S. Manganese(I) Complexes with Metal-to-Ligand Charge Transfer Luminescence and Photoreactivity. *Nat. Chem.* **2021**, *13* (10), 956–962. https://doi.org/10.1038/s41557-021-00744-9.
(80) East, N. R.; Naumann, R.; Förster, C.; Ramanan, C.; Diezemann, G.; Heinze, K. Oxidative Two-State Photoreactivity of a Manganese(IV) Complex Using near-Infrared Light. *Nat. Chem.* **2024**. https://doi.org/10.1038/s41557-024-01446-8.
(81) Ford, W. E.; Rodgers, M. A. J. Reversible Triplet-Triplet Energy Transfer within a Covalently Linked Bichromophoric Molecule. *J. Phys. Chem.* **1992**, *96* (7), 2917–2920. https://doi.org/10.1021/j100186a026.
(82) Tyson, D. S.; Bialecki, J.; Castellano, F. N. Ruthenium(II) Complex with a Notably Long Excited State Lifetime. *Chem. Commun.* **2000**, No. 23, 2355–2356. https://doi.org/10.1039/b007336i.
(83) Tyson, D. S.; Henbest, K. B.; Bialecki, J.; Castellano, F. N. Excited State Processes in Ruthenium(II)/Pyrenyl Complexes Displaying Extended Lifetimes. *J. Phys. Chem. A* **2001**, *105* (35), 8154–8161. https://doi.org/10.1021/jp011770f.
(84) Kerzig, C.; Goez, M. Combining Energy and Electron Transfer in a Supramolecular Environment for the "Green" Generation and Utilization of Hydrated Electrons through Photoredox Catalysis. *Chem. Sci.* **2016**, *7* (6), 3862–3868. https://doi.org/10.1039/C5SC04800A.
(85) Deng, F.; Lazorski, M. S.; Castellano, F. N. Photon Upconversion Sensitized by a Ru(II)-Pyrenyl Chromophore. *Philos. Trans. R. Soc. Math. Phys. Eng. Sci.* **2015**, *373* (2044), 20140322. https://doi.org/10.1098/rsta.2014.0322.
(86) Ghosh, I.; Shaikh, R. S.; König, B. Sensitization-Initiated Electron Transfer for Photoredox Catalysis. *Angew. Chem. Int. Ed.* **2017**, *56* (29), 8544–8549. https://doi.org/10.1002/anie.201703004.
(87) Coles, M. S.; Quach, G.; Beves, J. E.; Moore, E. G. A Photophysical Study of Sensitization-Initiated Electron Transfer: Insights into the Mechanism of Photoredox Activity. *Angew. Chem. Int. Ed.* **2020**, *59* (24), 9522–9526. https://doi.org/10.1002/anie.201916359.
(88) Yu, W.; Wang, X.-Y.; Li, J.; Li, Z.-T.; Yan, Y.-K.; Wang, W.; Pei, J. A Photoconductive Charge-Transfer Crystal with Mixed-Stacking Donor–Acceptor Heterojunctions within the Lattice. *Chem Commun* **2013**, *49* (1), 54–56. https://doi.org/10.1039/C2CC37655E.
(89) Mallon, M.; Dutt, S.; Schrader, T.; Crowley, P. B. Protein Camouflage: Supramolecular Anion Recognition by Ubiquitin. *ChemBioChem* **2016**, *17* (8), 774–783. https://doi.org/10.1002/cbic.201500477.
(90) Karakostas, N.; Mavridis, I. M.; Seintis, K.; Fakis, M.; Koini, E. N.; Petsalakis, I. D.; Pistolis, G. Highly Efficient and Unidirectional Energy Transfer within a Tightly Self-Assembled Host–Guest Multichromophoric Array. *Chem. Commun.* **2014**, *50* (11), 1362–1365. https://doi.org/10.1039/C3CC48076C.
(91) Rambabu, D.; Pradeep, C. P.; Dhir, A. Nickel–Sodium Pyrene Tetrasulfonic Acid Based Co-Ordination Polymer as Fluorescent Template for Recognition of Azo Dyes. *Sens. Actuators B Chem.* **2016**, *225*, 586–592. https://doi.org/10.1016/j.snb.2015.11.055.
(92) Hasegawa, M.; Yamasaki, Y.; Sonta, N.; Shindo, Y.; Sugimura, T.; Kitahara, A. Clustering of Aerosol OT Reversed Micelles As Studied by Nonradiative Energy Transfer of Solubilized Probes. *J. Phys. Chem.* **1996**, *100* (38), 15575–15580. https://doi.org/10.1021/jp961528m.

(93) Feng, X.; Wang, X.; Redshaw, C.; Tang, B. Z. Aggregation Behaviour of Pyrene-Based Luminescent Materials, from Molecular Design and Optical Properties to Application. *Chem. Soc. Rev.* **2023**, *52* (19), 6715–6753. https://doi.org/10.1039/D3CS00251A.
(94) Balzani, V.; Campagna, S. *Photochemistry and Photophysics of Coordination Compounds I*; Topics in Current Chemistry; Springer Berlin Heidelberg Springer e-books: Berlin, Heidelberg, 2007.
(95) Montalti, M.; Credi, A.; Prodi, L.; Gandolfi, M. T. *Handbook of Photochemistry*, 3rd ed.; CRC Press, 2006. https://doi.org/10.1201/9781420015195.
(96) Tanwar, A. S.; Parui, R.; Garai, R.; Chanu, M. A.; Iyer, P. K. Dual "Static and Dynamic" Fluorescence Quenching Mechanisms Based Detection of TNT via a Cationic Conjugated Polymer. *ACS Meas. Sci. Au* **2022**, *2* (1), 23–30. https://doi.org/10.1021/acsmeasuresciau.1c00023.
(97) Genovese, D.; Cingolani, M.; Rampazzo, E.; Prodi, L.; Zaccheroni, N. Static Quenching upon Adduct Formation: A Treatment without Shortcuts and Approximations. *Chem. Soc. Rev.* **2021**, *50* (15), 8414–8427. https://doi.org/10.1039/D1CS00422K.
(98) Thordarson, P. Determining Association Constants from Titration Experiments in Supramolecular Chemistry. *Chem Soc Rev* **2011**, *40* (3), 1305–1323. https://doi.org/10.1039/C0CS00062K.
(99) Brynn Hibbert, D.; Thordarson, P. The Death of the Job Plot, Transparency, Open Science and Online Tools, Uncertainty Estimation Methods and Other Developments in Supramolecular Chemistry Data Analysis. *Chem. Commun.* **2016**, *52* (87), 12792–12805. https://doi.org/10.1039/C6CC03888C.
(100) Bohne, C.; Abuin, E. B.; Scaiano, J. C. Characterization of the Triplet-Triplet Annihilation Process of Pyrene and Several Derivatives under Laser Excitation. *J. Am. Chem. Soc.* **1990**, *112* (11), 4226–4231. https://doi.org/10.1021/ja00167a018.
(101) Mori, Y.; Shinoda, H.; Nakano, T.; Kitagawa, T. Formation and Decay Behaviors of Laser-Induced Transient Species from Pyrene Derivatives 1. Spectral Discrimination and Decay Mechanisms in Aqueous Solution. *J. Phys. Chem. A* **2002**, *106* (48), 11743–11749. https://doi.org/10.1021/jp020332l.
(102) Mori, Y.; Shinoda, H.; Nakano, T.; Kitagawa, T. Formation and Decay Behaviors of Laser-Induced Transient Species from Pyrene Derivatives 2. Micellar Effects. *J. Phys. Chem. A* **2002**, *106* (48), 11750–11759. https://doi.org/10.1021/jp020333d.
(103) Bertrams, M.-S.; Kerzig, C. Converting *p* -Terphenyl into a Novel Organo-Catalyst for LED-Driven Energy and Electron Transfer Photoreactions in Water. *Chem. Commun.* **2021**, *57* (55), 6752–6755. https://doi.org/10.1039/D1CC01947C.
(104) Strieth-Kalthoff, F.; Henkel, C.; Teders, M.; Kahnt, A.; Knolle, W.; Gómez-Suárez, A.; Dirian, K.; Alex, W.; Bergander, K.; Daniliuc, C. G.; Abel, B.; Guldi, D. M.; Glorius, F. Discovery of Unforeseen Energy-Transfer-Based Transformations Using a Combined Screening Approach. *Chem* **2019**, *5* (8), 2183–2194. https://doi.org/10.1016/j.chempr.2019.06.004.
(105) Wasserman, H. H.; Ives, J. L. Singlet Oxygen in Organic Synthesis. *Tetrahedron* **1981**, *37* (10), 1825–1852. https://doi.org/10.1016/S0040-4020(01)97932-3.
(106) DeRosa, M. Photosensitized Singlet Oxygen and Its Applications. *Coord. Chem. Rev.* **2002**, *233–234*, 351–371. https://doi.org/10.1016/S0010-8545(02)00034-6.
(107) Ogilby, P. R. Singlet Oxygen: There Is Indeed Something New under the Sun. *Chem. Soc. Rev.* **2010**, *39* (8), 3181. https://doi.org/10.1039/b926014p.
(108) Pibiri, I.; Buscemi, S.; Palumbo Piccionello, A.; Pace, A. Photochemically Produced Singlet Oxygen: Applications and Perspectives. *ChemPhotoChem* **2018**, *2* (7), 535–547. https://doi.org/10.1002/cptc.201800076.
(109) Ghogare, A. A.; Greer, A. Using Singlet Oxygen to Synthesize Natural Products and Drugs. *Chem. Rev.* **2016**, *116* (17), 9994–10034. https://doi.org/10.1021/acs.chemrev.5b00726.
(110) Wang, Y.; Lin, Y.; He, S.; Wu, S.; Yang, C. Singlet Oxygen: Properties, Generation, Detection, and Environmental Applications. *J. Hazard. Mater.* **2024**, *461*, 132538. https://doi.org/10.1016/j.jhazmat.2023.132538.
(111) McNeill, K.; Canonica, S. Triplet State Dissolved Organic Matter in Aquatic Photochemistry: Reaction Mechanisms, Substrate Scope, and Photophysical Properties. *Environ. Sci. Process. Impacts* **2016**, *18* (11), 1381–1399. https://doi.org/10.1039/C6EM00408C.

(112) Losev, A. P.; Byteva, I. M.; Gurinovich, G. P. Singlet Oxygen Luminescence Quantum Yields in Organic Solvents and Water. *Chem. Phys. Lett.* **1988**, *143* (2), 127–129. https://doi.org/10.1016/0009-2614(88)87025-8.
(113) Kraljić, I.; Mohsni, S. E. A New Method for the Detection of Singlet Oxygen in Aqueous Solutions. *Photochem. Photobiol.* **1978**, *28* (4–5), 577–581. https://doi.org/10.1111/j.1751-1097.1978.tb06972.x.
(114) Garcìa-Fresnadillo, D.; Georgiadou, Y.; Orellana, G.; Braun, A. M.; Oliveros, E. Singlet-Oxygen ($^1\Delta_g$) Production by Ruthenium(II) Complexes Containing Polyazaheterocyclic Ligands in Methanol and in Water. *Helv. Chim. Acta* **1996**, *79* (4), 1222–1238. https://doi.org/10.1002/hlca.19960790428.
(115) Galkin, K. I.; Ananikov, V. P. When Will 5-Hydroxymethylfurfural, the "Sleeping Giant" of Sustainable Chemistry, Awaken? *ChemSusChem* **2019**, *12* (13), 2976–2982. https://doi.org/10.1002/cssc.201900592.
(116) Hu, L.; Lin, L.; Wu, Z.; Zhou, S.; Liu, S. Recent Advances in Catalytic Transformation of Biomass-Derived 5-Hydroxymethylfurfural into the Innovative Fuels and Chemicals. *Renew. Sustain. Energy Rev.* **2017**, *74*, 230–257. https://doi.org/10.1016/j.rser.2017.02.042.
(117) Heugebaert, T. S. A.; Stevens, C. V.; Kappe, C. O. Singlet-Oxygen Oxidation of 5-Hydroxymethylfurfural in Continuous Flow. *ChemSusChem* **2015**, *8* (10), 1648–1651. https://doi.org/10.1002/cssc.201403182.
(118) Nsubuga, A.; Mandl, G. A.; Capobianco, J. A. Investigating the Reactive Oxygen Species Production of Rose Bengal and Merocyanine 540-Loaded Radioluminescent Nanoparticles. *Nanoscale Adv.* **2021**, *3* (5), 1375–1381. https://doi.org/10.1039/D0NA00964D.
(119) Saito, I.; Inoue, K.; Matsuura, T. Occurence of the Singlet-Oxygen Mechanism in Photodynamic Oxidations of Guanosine*. *Photochem. Photobiol.* **1975**, *21* (1), 27–30. https://doi.org/10.1111/j.1751-1097.1975.tb06625.x.
(120) Fernandez, J. M.; Bilgin, M. D.; Grossweiner, L. I. Singlet Oxygen Generation by Photodynamic Agents. *J. Photochem. Photobiol. B* **1997**, *37* (1–2), 131–140. https://doi.org/10.1016/S1011-1344(96)07349-6.
(121) Xu, J.; Pelluau, T.; Monnereau, C.; Guari, Y.; Bonneviot, L.; Rodríguez-Pizarro, M.; Albela, B. Incorporation of Methylene Blue into Mesoporous Silica Nanoparticles for Singlet Oxygen Generation. *New J. Chem.* **2023**, *47* (4), 1861–1871. https://doi.org/10.1039/D2NJ04835C.
(122) Guerra Díaz, D.; Mariño-Ocampo, N.; Kabanov, V.; Heyne, B.; Andrade-Villalobos, F.; Fierro, A.; Fuentealba, D. Extraordinary Control of Photosensitized Singlet Oxygen Generation by Acyclic Cucurbituril-like Containers. *J. Phys. Chem. B* **2023**, *127* (15), 3443–3451. https://doi.org/10.1021/acs.jpcb.3c00583.
(123) Usui, Y. Determination of Quantum Yield of Singlet Oxygen Formation by Photosensitization. *Chem. Lett.* **1973**, *2* (7), 743–744. https://doi.org/10.1246/cl.1973.743.
(124) Amat-Guerri, F.; López-González, M. M. C.; Martínez-Utrilla, R.; Sastre, R. Singlet Oxygen Photogeneration by Ionized and Un-Ionized Derivatives of Rose Bengal and Eosin Y in Diluted Solutions. *J. Photochem. Photobiol. Chem.* **1990**, *53* (2), 199–210. https://doi.org/10.1016/1010-6030(90)87124-T.
(125) Zhang, Y.; Ye, C.; Li, S.; Ding, A.; Gu, G.; Guo, H. Eosin Y-Catalyzed Photooxidation of Triarylphosphines under Visible Light Irradiation and Aerobic Conditions. *RSC Adv.* **2017**, *7* (22), 13240–13243. https://doi.org/10.1039/C6RA25469A.
(126) Wilkinson, F.; Helman, W. P.; Ross, A. B. Rate Constants for the Decay and Reactions of the Lowest Electronically Excited Singlet State of Molecular Oxygen in Solution. An Expanded and Revised Compilation. *J. Phys. Chem. Ref. Data* **1995**, *24* (2), 663–677. https://doi.org/10.1063/1.555965.
(127) Caculated with the Price from "BLDpharm", Accessed March 08, 2024.
(128) Skolia, E.; Gkizis, P. L.; Nikitas, N. F.; Kokotos, C. G. Photochemical Aerobic Oxidation of Sulfides to Sulfoxides: The Crucial Role of Wavelength Irradiation. *Green Chem.* **2022**, *24* (10), 4108–4118. https://doi.org/10.1039/D2GC00799A.
(129) Jensen, F.; Greer, A.; Clennan, E. L. Reaction of Organic Sulfides with Singlet Oxygen. A Revised Mechanism. *J. Am. Chem. Soc.* **1998**, *120* (18), 4439–4449. https://doi.org/10.1021/ja973782d.

(130) Srour, H.; Jalkh, J.; Le Maux, P.; Chevance, S.; Kobeissi, M.; Simonneaux, G. Asymmetric Oxidation of Sulfides by Hydrogen Peroxide Catalyzed by Chiral Manganese Porphyrins in Water/Methanol Solution. *J. Mol. Catal. Chem.* **2013**, *370*, 75–79. https://doi.org/10.1016/j.molcata.2012.12.016.
(131) Zhang, G.; Tan, H.; Chen, W.; Shen, H. C.; Lu, Y.; Zheng, C.; Xu, H. Synthesis of NH-Sulfoximines by Using Recyclable Hypervalent Iodine(III) Reagents under Aqueous Micellar Conditions. *ChemSusChem* **2020**, *13* (5), 922–928. https://doi.org/10.1002/cssc.201903430.
(132) Adamson, A. W.; Waltz, W. L.; Zinato, Edoardo.; Watts, D. W.; Fleischauer, P. D.; Lindholm, R. D. Photochemistry of Transition-Metal Coordination Compounds. *Chem. Rev.* **1968**, *68* (5), 541–585. https://doi.org/10.1021/cr60255a002.
(133) Endicott, J. F.; Ramasami, T.; Tamilarasan, R.; Lessard, R. B.; Ryu, C. K.; Brubaker, G. R. Structure and Reactivity of the Metal-Centered Transition Metal Excited States. *Coord. Chem. Rev.* **1987**, *77*, 1–87. https://doi.org/10.1016/0010-8545(87)85032-4.
(134) Soupart, A.; Alary, F.; Heully, J.-L.; Elliott, P. I. P.; Dixon, I. M. Theoretical Study of the Full Photosolvolysis Mechanism of $[Ru(Bpy)_3]^{2+}$: Providing a General Mechanistic Roadmap for the Photochemistry of $[Ru(N\hat{}N)_3]^{2+}$ -Type Complexes toward Both Cis and Trans Photoproducts. *Inorg. Chem.* **2020**, *59* (20), 14679–14695. https://doi.org/10.1021/acs.inorgchem.0c01843.
(135) Kavarnos, G. J.; Turro, N. J. Photosensitization by Reversible Electron Transfer: Theories, Experimental Evidence, and Examples. *Chem. Rev.* **1986**, *86* (2), 401–449. https://doi.org/10.1021/cr00072a005.
(136) Goez, M. In *Annual Reports on NMR Spectroscopy*; Elsevier: Amsterdam, 2009; pp 77–147.
(137) McLauchlan, K. A.; Steiner, U. E. Invited Article: The Spin-Correlated Radical Pair as a Reaction Intermediate. *Mol. Phys.* **1991**, *73* (2), 241–263. https://doi.org/10.1080/00268979100101181.
(138) Haselbach, E.; Vauthey, E.; Suppan, P. Comparison of Photoinduced Electron Transfer Reactions of Aromatic Carbonyl vs. Cyano Compounds with Electron Donors in Condensed Phase:The Importance. *Tetrahedron* **1988**, *44* (24), 7335–7344. https://doi.org/10.1016/S0040-4020(01)86228-1.
(139) Olmsted, John.; Meyer, T. J. Factors Affecting Cage Escape Yields Following Electron-Transfer Quenching. *J. Phys. Chem.* **1987**, *91* (6), 1649–1655. https://doi.org/10.1021/j100290a071.
(140) Troian-Gautier, L.; Turlington, M. D.; Wehlin, S. A. M.; Maurer, A. B.; Brady, M. D.; Swords, W. B.; Meyer, G. J. Halide Photoredox Chemistry. *Chem. Rev.* **2019**, *119* (7), 4628–4683. https://doi.org/10.1021/acs.chemrev.8b00732.
(141) Venturi, M.; Emmi, S.; Fuochi, P. G.; Mulazzani, Q. G. Nucleophilic Addition of .Alpha.-Hydroxyalkyl Radicals to Polypyridyl Complexes of Chromium(III), Cobalt(III), Rhodium(III), and Ruthenium(II) in Aqueous Solution. *J. Phys. Chem.* **1980**, *84* (17), 2160–2166. https://doi.org/10.1021/j100454a011.
(142) Ohno, Takeshi.; Yoshimura, Akio.; Mataga, Noboru. Bell-Shaped Energy-Gap Dependence of Backward Electron Transfer Occurring within Geminate Radical Pairs Produced by Quenching of Ruthenium(II) Polypyridine Complexes by Aromatic Amines. *J. Phys. Chem.* **1990**, *94* (12), 4871–4876. https://doi.org/10.1021/j100375a023.
(143) Hai-Xia, Y.; Hu-Xiang, P.; Yan-Lin, W.; Jian-Feng, Z.; Wen-Bo, D.; 复旦大学环境科学与工程系, 上海 200433; Department of Environmental Science and Engineering, Fudan University, Shanghai 200433, P. R. China; 海军医学研究所, 上海 200433,Institute of Naval Medicine, Shanghai 200433, P. R. China. Laser Flash Photolysis Mechanism of Pyrenetetrasulfonate in Aqueous Solution. *Acta Phys.-Chim. Sin.* **2012**, *28* (04), 957–962. https://doi.org/10.3866/PKU.WHXB201202203.
(144) Kitzmann, W. R.; Bertrams, M.-S.; Boden, P.; Fischer, A. C.; Klauer, R.; Sutter, J.; Naumann, R.; Förster, C.; Niedner-Schatteburg, G.; Bings, N. H.; Hunger, J.; Kerzig, C.; Heinze, K. Stable Molybdenum(0) Carbonyl Complex for Upconversion and Photoredox Catalysis. *J. Am. Chem. Soc.* **2023**, *145* (30), 16597–16609. https://doi.org/10.1021/jacs.3c03832.
(145) Pellegrin, Y.; Odobel, F. Sacrificial Electron Donor Reagents for Solar Fuel Production. *Comptes Rendus Chim.* **2017**, *20* (3), 283–295. https://doi.org/10.1016/j.crci.2015.11.026.
(146) Kerzig, C.; Guo, X.; Wenger, O. S. Unexpected Hydrated Electron Source for Preparative Visible-Light Driven Photoredox Catalysis. *J. Am. Chem. Soc.* **2019**, *141* (5), 2122–2127. https://doi.org/10.1021/jacs.8b12223.

(147) Khnayzer, R. S.; Thoi, V. S.; Nippe, M.; King, A. E.; Jurss, J. W.; El Roz, K. A.; Long, J. R.; Chang, C. J.; Castellano, F. N. Towards a Comprehensive Understanding of Visible-Light Photogeneration of Hydrogen from Water Using Cobalt(II) Polypyridyl Catalysts. *Energy Env. Sci* **2014**, *7* (4), 1477–1488. https://doi.org/10.1039/C3EE43982H.
(148) Giedyk, M.; Narobe, R.; Weiß, S.; Touraud, D.; Kunz, W.; König, B. Photocatalytic Activation of Alkyl Chlorides by Assembly-Promoted Single Electron Transfer in Microheterogeneous Solutions. *Nat. Catal.* **2019**, *3* (1), 40–47. https://doi.org/10.1038/s41929-019-0369-5.
(149) Guttentag, M.; Rodenberg, A.; Kopelent, R.; Probst, B.; Buchwalder, C.; Brandstätter, M.; Hamm, P.; Alberto, R. Photocatalytic H $_2$ Production with a Rhenium/Cobalt System in Water under Acidic Conditions. *Eur. J. Inorg. Chem.* **2012**, *2012* (1), 59–64. https://doi.org/10.1002/ejic.201100883.
(150) Logan, S. R. Effects of Ionic Strength on the Rates of Reaction between Ions in Solution. *Trans. Faraday Soc.* **1967**, *63*, 3004. https://doi.org/10.1039/tf9676303004.
(151) Davies, M. B.; Austin, J.; Partridge, D. A. *Vitamin C: Its Chemistry and Biochemistry*; Royal society of chemistry paperbacks; The Royal society of chemistry: Cambridge, 1991.
(152) Bryden, M. A.; Millward, F.; Matulaitis, T.; Chen, D.; Villa, M.; Fermi, A.; Cetin, S.; Ceroni, P.; Zysman-Colman, E. Moving Beyond Cyanoarene Thermally Activated Delayed Fluorescence Compounds as Photocatalysts: An Assessment of the Performance of a Pyrimidyl Sulfone Photocatalyst in Comparison to 4CzIPN. *J. Org. Chem.* **2023**, *88* (10), 6364–6373. https://doi.org/10.1021/acs.joc.2c01137.
(153) Nakajima, M.; Fava, E.; Loescher, S.; Jiang, Z.; Rueping, M. Photoredox-Catalyzed Reductive Coupling of Aldehydes, Ketones, and Imines with Visible Light. *Angew. Chem. Int. Ed.* **2015**, *54* (30), 8828–8832. https://doi.org/10.1002/anie.201501556.
(154) Huh, H. H.; Lee, Y. J.; Anita, Y.; Woo, S. K. Visible-Light-Photocatalyzed Pinacol Coupling in Water. *Asian J. Org. Chem.* **2024**, e202300591. https://doi.org/10.1002/ajoc.202300591.
(155) Naumann, R.; Goez, M. How the Sustainable Solvent Water Unleashes the Photoredox Catalytic Potential of Ruthenium Polypyridyl Complexes for Pinacol Couplings. *Green Chem.* **2019**, *21* (16), 4470–4474. https://doi.org/10.1039/C9GC02069A.
(156) Bai, C.; Tian, B.; Zhao, T.; Huang, Q.; Wang, Z. Cyclodextrin-Catalyzed Organic Synthesis: Reactions, Mechanisms, and Applications. *Molecules* **2017**, *22* (9), 1475. https://doi.org/10.3390/molecules22091475.